Simulations of column-averaged CO_2 and CH_4 using the NIES TM with a hybrid sigma–isentropic (σ–θ) vertical coordinate

D.A. Belikov[1], S. Maksyutov[1], V. Sherlock[2], S. Aoki[3], N.M. Deutscher[4,5], S. Dohe[6], D. Griffith[5], E. Kyro[7], I. Morino[1], T. Nakazawa[3], J. Notholt[4], M. Rettinger[6], M. Schneider[6], R. Sussmann[6], G.C. Toon[8], P.O. Wennberg[8], D. Wunch[8]

[1] {National Institute for Environmental Studies, Tsukuba, Ibaraki, Japan}

[2] {Department of Atmospheric Research, National Institute of Water and Atmospheric Research, Wellington, New Zealand}

[3] {Center for Atmospheric and Oceanic Studies, Graduate School of Science, Tohoku University, Sendai, Japan}

[4] {Institute of Environmental Physics, University of Bremen, Bremen, Germany}

[5] {School of Chemistry, University of Wol longong, Wollongong, Australia}

[6] {Institute for Meteorology and Climate Research, Karlsruhe Institute of Technology, Karlsruhe, Germany}

[7] {Arctic Research Center, Finnish Meteorological Institute, Helsinki, Finland}

[8] {Department of Earth Science and Engineering, California Institute of Technology, Pasadena, CA, USA}

Correspondence to: Dmitry Belikov, email: dmitry.belikov @ nies.go.jp

Abstract. *We have developed an improved version of the National Institute for Environmental Studies (NIES) three-dimensional chemical transport model (TM) designed for accurate tracer transport simulations in the stratosphere, given the use of a hybrid sigma–isentropic (σ–θ) vertical coordinate that employed both terrain following and isentropic parts switched smoothly around the tropopause. The air-ascending rate was derived from the effective heating rate and was used to simulate vertical motion in the isentropic part of the grid (above level 350 K), which was adjusted to fit to the observed age of the air in the stratosphere. Multi-annual simulations were conducted using NIES TM to evaluate vertical profiles and dry-air column-averaged mole fractions of CO_2 and CH_4. Comparisons with balloon-borne observations over Sanriku (Japan) in 2000–2007 revealed that the tracer transport simulations in the upper troposphere and lower stratosphere are performed with accuracies of ~5% for CH_4 and SF_6, and ~1% for CO_2 compared with the observed volume-mixing ratios. The simulated column-averaged dry air mole fractions of atmospheric carbon dioxide (XCO_2) and methane (XCH_4) were evaluated against daily ground-based high-resolution Fourier Transform Spectrometer (FTS) observations measured at twelve sites of the Total Carbon Column Observing Network (TCCON) (Bialystok, Bremen, Darwin, Garmisch, Izaña, Lamont, Lauder, Orleans, Park Falls, Sodankylä, Tsukuba, and Wollongong) between January 2009 and January 2011. The comparison shows the model's ability to reproduce the site-dependent seasonal cycles as observed by TCCON, with correlation coefficients typically on the order 0.8–0.9 and 0.4–0.8 for XCO_2 and XCH_4, respectively, and mean model biases of ±0.2% and ±0.5%, excluding Sodankylä, where strong biases are found. The capturing of tracer total column mole fractions is strongly dependent on the model's ability to reproduce seasonal variations in tracer concentrations in the planetary boundary layer (PBL). We found a marked difference in the model's ability to reproduce near-surface concentrations at sites located some distance from multiple emission sources and where high emissions play a notable role in the tracer's budget. Comparisons with aircraft observations over Surgut (West Siberia), in an area with high emissions of methane from wetlands, show contrasting model performance in the PBL and in the free troposphere. Thus, the PBL is another critical region for simulating the tracer total column mole fractions.*

1. Introduction

Carbon dioxide (CO_2) and methane (CH_4) are the greenhouse gases that contribute the most to global warming (IPCC, 2007). Recent studies of global sources and sinks of greenhouse gases, and their concentrations and distributions, have been based mainly on *in situ* surface measurements (GLOBALVIEW-CH4, 2009; GLOBALVIEW-CO2, 2010). The diurnal and seasonal "rectifier effect", the covariance between surface fluxes and the strength of vertical mixing, and the proximity of local sources and sinks to surface measurement sites all have an influence on the measured and simulated concentrations, and complicate the interpretation of results (Denning et al., 1996; Gurney et al., 2004; Baker et al., 2006).

In contrast, column-averaged dry-air mole fractions (DMFs; denoted XG for gas G) are much less sensitive to the vertical redistribution of the tracer within the atmospheric column (e.g. due to variations in planetary boundary layer (PBL) height) and are more directly related to the underpinning surface fluxes than are near-surface concentrations (Yang et al., 2007). Thus, column-averaged measurements and simulations are expected to be very useful for improving our understanding of the carbon cycle (Yang et al., 2007; Keppel-Aleks et al., 2011; Wunch et al., 2011).

The Short-Wave InfraRed (SWIR) measurements from the SCIAMACHY imaging spectrometer onboard the ENVISAT satellite (Bovensmann et al., 2001) and the Japanese Greenhouse gases Observing SATellite (GOSAT) (Yokota et al., 2009) show some usefulness in determining the dry-air column-averaged mole fractions of carbon dioxide (XCO_2) and methane (XCH_4) (Bergamaschi et al., 2007, 2009; Bloom et al., 2010). However, the GOSAT retrieval algorithms are under continuing development and require reliable data for evaluation. One appropriate way to validate GOSAT is to use ground-based high-resolution Fourier Transform Spectrometer (FTS) observations from the Total Carbon Column Observing Network (TCCON) (Butz et al., 2011; Morino et al., 2011; Parker et al., 2011; Wunch et al., 2011). Ground-based FTS observations of the absorption of direct sunlight by atmospheric gases in the near-infrared (NIR) spectral region provide accurate measurements of the total columns of greenhouse gases (Wunch et al., 2010). Due to the limited number of TCCON sites, there is a relatively uneven spatial distribution of measurements, and measurements are not continuous because they depend on the cloud conditions (Wunch et al., 2011). As a result, there are notable temporal and spatial gaps in the data coverage, particularly at high latitudes and over heavily clouded areas such as South America, Africa, and Asia; in such areas, model data can be used (Parker et al., 2011).

The synoptic and seasonal variabilities in XCO_2 and XCH_4 are driven mainly by changes in

surface pressure, the tropospheric volume-mixing ratio (VMR) and the stratospheric concentration, which is affected in turn by changes in tropopause height. The effects of variations in tropopause height are more pronounced with increasing contrast between stratospheric and tropospheric concentrations; i.e., the influence is greater for CH_4 than for CO_2 due to CH_4 oxidation by O(1D), OH, and Cl in the stratosphere. A 30-ppbv change in tropospheric CH_4 or a 30-hPa change in tropopause height would produce a ~1.5% variation in sea level XCH_4 (Washenfelder et al., 2003).

A precision of 2.5 ppmv (better than 1%) for CO_2 (Rayner and O'Brien, 2001) and 1%–2% for CH_4 (Meirink et al., 2006) for monthly mean column-integrated concentrations on a regional scale is needed to reduce uncertainties in predictions of the carbon cycle. The target requirement formulated for the candidate Earth Explorer mission A-SCOPE mission is 0.02 PgC/yr per 106 km^2 or 0.1 ppmv (Ingmann, 2009; Houweling et al., 2010). Transport-model-induced flux uncertainties that exceed the target requirement could also limit the overall performance of CO_2 missions such as GOSAT. However, the model accuracy requirement may depend on the measurement sensitivity (averaging kernel) for different tracers. If the measurement has little or no sensitivity to the tracer VMR in a given altitude region, then the accuracy of the model tracer concentrations in that region is irrelevant. A key element in accurately determining XCO_2 and XCH_4 is to obtain precise simulations of tracers throughout the atmosphere, including the stratosphere as well as the PBL.

Hall et al. (1999) suggested that many chemical transport models (CTMs) demonstrate some common failings of model transport in the stratosphere. The difficulty of accurately representing dynamical processes in the upper troposphere (UT) and lower stratosphere (LS) has been highlighted in recent studies (Mahowald et al., 2002; Waugh and Hall, 2002; Monge-Sanz et al., 2007). While there are many contributing factors in this regard, the principal factors affecting model performance in vertical transport are meteorological data and the vertical grid layout (Monge-Sanz et al., 2007).

The use of different meteorological fields in driving chemical transport models can lead to diverging distributions of chemical species in the upper troposphere/lower stratosphere (UTLS) region (Douglass et al., 1999). Several studies based on multi-year CTM simulations have shown that vertical winds directly supplied from analyses can result in an over-prediction of the strength of the stratospheric circulation and an under-prediction of the age of air (Chipperfield, 2006; Monge-Sanz et al., 2007). On the isentropic grid, the diabatic heating rate can substitute for the analysed vertical velocity. A radiation scheme or recalculated radiation data can be implemented to resolve some of the problems of vertical winds from assimilated data products. Weaver et al. (1993) found that the use of a radiative scheme for long-term simulations gave a better representation of the meridional circulation,

compared with simulations using the analysed vertical winds.

The isentropic vertical coordinate system has notable advantages over other types of coordinate systems, such as height, pressure, and "sigma" (Arakawa and Moorthi, 1988; Hsu, 1990), due to its ability to minimize vertical truncation and the non-existence of vertical motion under adiabatic conditions, except for diabatic heating (Bleck, 1978; Kalnay, 2002). These advantages result in reduced finite difference errors in sloping frontal surfaces, where pressure or *z*-coordinates tend to have large errors associated with poorly resolved vertical motion. The implementation of an isentropic coordinate with a radiation scheme helps to avoid erroneous vertical dispersion and enables the accurate calculation of vertical transport in the UTLS region (Mahowald et al., 2002; Chipperfield, 2006).

The aim of this study is to develop a NIES TM version with an improved tracer transport simulation in the stratosphere by implementing a sigma–isentropic coordinate system with an air-ascending rate derived from the effective heating rate, in order to obtain a more accurate simulation of atmospheric CO_2 and CH_4 profiles, and corresponding column-averaged concentration. The remainder of the paper is organized as follows. The model modifications are described in Section 2, and Section 3 presented results i.e., evaluation the modelled age of the air and validation the CO_2, CH_4, and SF_6 vertical profiles by comparison against balloon-borne *in situ* observations in the stratosphere. Also examined is the model's performance in reproducing the near-surface concentration and free-troposphere vertical profiles of CH_4. XCO_2 and XCH_4 simulated by NIES TM are compared with daily FTS observations at twelve TCCON sites between January 2009 and January 2011. Finally, a discussion (Section 4) and conclusions (Section 5) are provided.

2. Model description

This section describes the formulation of the NIES model version (denoted NIES-08.1i) used in this paper. Belikov et al. (2011) described the main model features, such as the flux-form dynamical core with a third-order van Leer advection scheme, a reduced latitude–longitude grid, a horizontal flux-correction method (necessary for mass conservation) and turbulence parameterization. However, the present paper focuses on the recently incorporated hybrid sigma–isentropic vertical coordinate and a change in the meteorological dataset used to drive the model.

2.1. Sigma–isentropic vertical coordinate

Previous NIES transport model versions with sigma–pressure and hybrid sigma–pressure vertical coordinate systems do not fully accommodate chemical and dynamical processes in the stratosphere, which results in the model failing to reproduce vertical tracer profiles. To overcome this issue, one can use climatological values of CO_2 and CH_4 in the stratosphere (Eguchi et al., 2010). However, this approach does not account for year-to-year VMR variation and can distort the meridional mass circulation in long-term simulations.

It was previously thought that because potential temperature under adiabatic motion is individually conserved, it could be used as an ideal vertical coordinate. However, in several studies that have been published since the first successful integration of hydrostatic equations in isentropic coordinates performed by Eliassen and Raustein (1968), a number of disadvantages have been revealed. Many of them relate to the fact that isentropes intersect the Earth's surface. The combined hybrid vertical coordinate system consisted of the θ coordinate in the free atmosphere (where the air motion is quasi-adiabatic) with a σ terrain-following system near the surface, which helps to avoid problems with the θ vertical coordinate (Bleck, 1978).

Hence, we follow the general methodology of Hsu and Arakawa (1990) and Konor and Arakawa (1997), and use the σ–θ hybrid sigma–isentropic coordinate that is isentropic in the UTLS region but terrain-following in the free troposphere. The coordinates switch smoothly near the tropopause level, as follows:

$$\sigma = \begin{cases} \left(P + \dfrac{\Delta P}{(\zeta - \theta)} \Delta\theta \right) \dfrac{1}{P_S}, & if\ \theta \geq \theta_T, \\ 1 - \dfrac{(P_S - P)(1 - \sigma_\theta)}{(P_S - P_\theta)}, & if\ \theta < \theta_T; \end{cases} \quad (1)$$

where ζ denotes the level of the sigma–isentropic grid as described in Table 1, P and P_s are atmospheric pressure and surface atmospheric pressure respectively, $\theta = T\left(P_S / P\right)^{\left(R/c_p\right)}$ is potential temperature, T depicts temperature, R is the molar gas constant, c_p is the specific heat for a constant pressure, σ_θ and P_θ are "sigma" and pressure at the level θ_T, respectively. We set $\theta_T = 350K$ to ensure that isentropes do not intersect the Earth's surface.

2.2. Simulation of upward motion in the stratosphere

To calculate vertical transport in the θ-coordinate domain of the hybrid sigma–isentropic coordinate, we use precalculated heating rates. Unlike the SLIMCAT model, which has an embedded diagnostic radiation scheme to calculate heating rates (Chipperfield, 2006), the NIES model interpolates the climatological heating rate at every meteorology data update step (3h) at every model cell of sigma–isentropic grid using 2D monthly distribution of atmospheric reanalysis heating rate (see Section 2.3).

The most problematic region in modelling vertical transport is a level around the tropopause transition region known as the Tropical Tropopause Layer (TTL). Radiative heating in the TTL is a result of heating from the absorption of infrared radiation by ozone and carbon dioxide, balanced by infrared cooling, mainly from water vapour (Thuburn and Craig, 2002). The level termed as the 'stagnation surface' (Sherwood and Dessler, 2003) occurs where the total heating rate $Q_{total} = 0$, and is demarcated by net cooling below and net heating above. The height of this transition level is almost constantly around $\theta = 360\ K$ (≈15 km, 125 hPa) (Gettelman et al., 2004; Folkins et al., 1999). There is some variability in the level of $Q_{total} = 0$; e.g., ±500 m between different locations and seasons; ±400 m for individual profiles (Gettelman et al., 2004).

Among other aspects of Troposphere-to-Stratosphere Transport (TST) that are not adequately addressed, it is unclear how air parcels overcome the vertical gap between the main convective outflow around 350 K and the level with significant heating rates (Konopka et al., 2007). In some models, erroneous spurious meteorology, a diffusive numerical scheme (Eluszkiewicz et al., 2000), or extra vertical motion due to the implementation of vertical transport misrepresenting the adiabatic conditions are responsible for extra artificial mixing in this region, thereby obscuring the vertical transport problem.

In isentropic coordinates, the impact of such erroneous effects is significantly reduced. As a result, the use of a simulated heating rate leads to insufficient TST of tracers through the TTL. When

models are unable to resolve a process explicitly, it is necessary to implement a parameterization to improve the simulation. Thus, Konopka et al. (2007) showed that more realistic tracer distributions are obtained by implementing the mixing parameterisation into a Chemical Lagrangian Model of the Stratosphere (CLaMS) with an isentropic vertical coordinate. Induced vertical mixing, driven mainly by vertical shear in the tropical flanks of subtropical jets, has been cited in explaining the upward transport of trace species from the main convective outflow to the tropical tropopause around 380 K (Konopka et al., 2007).

The total diabatic heating rates of different reanalysis products can produce dissimilar results (Fueglistaler et al., 2009). In our work, we implemented a scheme with additional transport in the TTL by increasing the air-ascending rate in the TTL, which was adjusted to fit the observed age of air in the stratosphere, as follows:

- For levels above 360 K (isentropic part of the vertical coordinate), the air-ascending rate was multiplied by 2.5.
- Constant vertical wind component (0.6 K/day) was set at the levels 180–40 hPa for tropical areas (15°S–15°N).

2.3. Meteorological data and vertical resolution

NIES TM is an off-line model driven by Japanese reanalysis data covering more than 30 years from 1 January 1979 (Onogi et al., 2007). The period of 1979–2004 is covered by the Japanese 25-year Reanalysis (JRA-25), which is a product of the Japan Meteorological Agency (JMA) and the Central Research Institute of Electric Power Industry (CRIEPI). After 2005, a real-time operational analysis, employing the same assimilation system as JRA-25, has been continued as the JMA Climate Data Assimilation System (JCDAS). The JRA-25/JCDAS dataset is distributed on Gaussian horizontal grid T106 (320 × 160) with 40 hybrid σ–p levels. The 6-hourly time step of JRA-25/JCDAS is coarser than the 3-hourly data from the National Centers for Environmental Prediction (NCEP) Global Forecast System (GFS) and Global Point Value (GPV) datasets, which were used in the previous model version (Belikov et al., 2011). However, with a better vertical resolution (40 levels on a hybrid σ–p grid versus 25 and 21 pressure levels for GFS and GPV, respectively) it is possible to implement a vertical grid with 32 levels (versus 25 levels used before), resulting in a more detailed resolution of the boundary layer and UTLS region (Table 1).

The 2D monthly distribution of the climatological heating rate used to calculate vertical transport

in the θ-coordinate domain of the hybrid sigma–isentropic coordinate is prepared from JRA-25 reanalysis data, which are provided as the sum of short- and long-wave components on pressure levels.

2.4. Turbulent diffusion and deep convection parameterization

The calculation of turbulent diffusion is similar to that described by Maksyutov et al. (2008). To separate the transport processes in the well-mixed near-surface layer and free troposphere, we used 3-hourly PBL height data taken from European Centre for Medium-Range Weather Forecasts (ECMWF) Interim Re-Analysis. Above the top of the PBL, the parameterisation of the turbulent diffusivity follows the approach used by Hack et al. (1993), who estimated free-troposphere diffusivity from local stability as a function of the Richardson number. Below the top of the PBL, the turbulent diffusivity is set to a constant value of 40 m^2s^{-1}, under the assumption that the boundary layer is well mixed.

Following Grell (1993), to simulate deep convection we used a Kuo-type penetrative cloud convection scheme including entrainment and detrainment processes on convective updrafts and downdrafts, as proposed by Tiedtke (1989). We calculated cumulus mass-flux from the detailed distribution of convection precipitation, using the method developed by Austin and Houze (1973), as first adopted by Feichter and Crutzen (1990). This approach is based on the fact that the amount of lifting air in an updraft core of a cumulus cell is related to precipitation, which it produces, and that the temperature excess and entrainment are reflected in its vertical development. Given the amount of the convective precipitation rate provided by the JRA-25/JCDAS dataset, the mass of air transported upward within the cells was computed from the conservation of moisture.

2.5. Model setup

In this paper, the performance of the new CTM in various configurations is investigated by running a series of experiments to study atmospheric tracer transport and the model's ability to reproduce the column-averaged dry air mole fractions of atmospheric CO_2 and CH_4. The model was run at a horizontal resolution of 2.5° × 2.5° and 32 vertical levels from the surface to 3 hPa, using three tracers: CO_2, CH_4, and sulphur hexafluoride (SF_6).

Forward model simulations were performed for SF_6 and CH_4 for 22 years (January 1988 to February 2011) using the simulation setup, initial distribution, fluxes, sinks, and chemical reactions (for CH_4) described in the Protocol for TransCom-CH_4 inter-comparison (Patra et al., 2011). For the CH_4

simulation, an inverse model-adjusted flux was used, obtained by optimising the surface fluxes of CH_4 using the LMDZ model for the period 1988–2005 (Bousquet et al., 2006). For the 2006–2011 fluxes, the average seasonal cycle was repeated. For the SF_6 simulation for the period 1988–2005, the annual mean SF_6 emission distributions at $1° \times 1°$ were taken from EDGAR 4.0 (2009), and the global totals were scaled by Levin et al. (2010). The 2005 distribution was used from 2006 onwards (Patra et al., 2011).

The simulation was started on 1 January 1988 using the initial 3D tracer distributions. This was prepared following a 10-year spin-up simulation by the Atmospheric General Circulation Model (AGCM)-based chemistry transport model with CH_4 and SF_6 concentrations at the South Pole of 1655 ppb and 1.95 ppt, respectively (Patra et al., 2011).

The CO_2 simulation was started on 1 January 2000 with the initial distribution derived from GLOBALVIEW-CO2 (2010) observations using prescribed fluxes from the Comprehensive Observation Network for Trace gases by AIrLiner (CONTRAIL) Transport Model Intercomparison (TMI) (Niwa et al., 2011), as follows:

1. Fossil fuel emissions are derived from the EDGAR-1998 distribution (Olivier and Berdowski, 2001) and the emission totals are scaled using the growth rate of the top 20 country-specific fossil fuel consumptions, as obtained from the Carbon Dioxide Information Analysis Center (CDIAC) (Boden et al., 2009).

2. The climatological inversion flux represents all non-fossil source/sink distributions over land and ocean, derived by inverse modelling with 12 TransCom3 models (Gurney et al., 2004) and from observational data obtained from GLOBALVIEW-CO2 at 87 sites during 1999–2001 (Miyazaki et al., 2008).

3. Results

The current model version has been used in several tracer transport studies and was evaluated through participation in transport model intercomparisons (Niwa et al., 2011; Patra et al., 2011). The model results of tracer transport simulations show good consistency with observations and other models in the near-surface layer and in the free troposphere. However, the model performance in the UTLS region has not been evaluated in detail.

3.1. Validation of the mean age of air in the stratosphere

The mean age of air is purely a transport diagnostic. Modellers are ultimately interested in accurately simulating the distribution of trace gases that are affected by both transport and photochemistry (Waugh and Hall, 2002). The accurate determination of the chemical constituents that are transported across the tropopause, which are strongly affected by synoptic-scale events and other small-scale mixing processes, is a major challenge for modern CTMs (Hall et al., 1999). In the stratosphere, the vertical transport of substances is very weak due to the almost adiabatic conditions. However, many models are unable to reproduce sufficiently weak transport, especially in the tropical lower stratosphere, because the model grid does not reflect the underlying constraint that the flow is almost isentropic, making the model transport vulnerable to numerical errors (Mahowald et al., 2002). Generally, models tend to have ages of air in the stratosphere that are too young and tend to propagate the signal upward from the troposphere into the lower stratosphere too quickly, especially in the tropics (Hall et al., 1999; Park et al., 1999). By implementing a hybrid sigma–isentropic vertical coordinate, the observed age of air is more accurately determined than when using a model that employs a hybrid pressure grid (Mahowald et al., 2002; Chipperfield, 2006; Monge-Sanz et al., 2007).

The mean age of air can be calculated from measured or modelled tracer concentrations that are conserved and that vary linearly with time (Waugh and Hall, 2002). Among several chemical species that approximately satisfy the criterion of linear variation, CO_2 and SF_6 are the most reliable compounds with which to derive the mean age, because they are very long-lived species and their annual mean concentrations have been increasing approximately linearly (Conway et al., 1994; Maiss et al., 1996). In spite of uncertainties due to nonlinearity in tropospheric growth rates and the neglect of photochemical processes (Waugh and Hall, 2002), estimates performed with CO_2, SF_6, and other tracers show rather good agreement.

In this paper, SF_6 is simulated to derive the mean age of the air in the upper troposphere and in

the lower stratosphere. The model was run for 22 years before the simulation results were analysed, because the age of stratospheric air was unchanged for the last 30 years (Engel et al., 2009).

Figure 1 shows the annual mean of the zonal-mean age of air obtained with NIES TM at an altitude of 20 km, together with the mean age values derived from CO_2 and SF_6 ER-2 aircraft observations (Andrews et al., 2001). Both the model and observation estimations of the mean age indicate values of approximately 1 year near the equator, large gradients in the subtropics, and values of around 4–5 years at high latitudes.

The vertical profiles of mean age derived from *in situ* measurements of CO_2 and SF_6 show that at all latitudes, the mean age of the air increased monotonically with height throughout the stratosphere, with only weak vertical gradients above 25 km (Figure 2). The model slightly overestimated the age of air in the tropics (Figure 2a) and underestimated it at middle and high latitudes (Figure 2b, c). The spikes in high-latitude profiles (Figure 2c) are due to the sampling of fragments of polar vortex air. Despite this, the general shape of the isopleths in Figure 3 is realistic and illustrates the balance of the meridional mass (Brewer–Dobson) circulation, which tends to increase latitudinal slopes, and isentropic mixing, which tends to decrease the slopes (Plumb and Ko, 1992).

3.2. Validation of CO_2, CH_4, and SF_6 vertical profiles in the stratosphere

To evaluate the model's ability to reproduce stratospheric transport, the simulated vertical profiles of CO_2, CH_4, and SF_6 were analysed and compared against balloon-borne observation data (Figure 4). The observed VMRs were derived from six individual profiles of balloon-borne measurements performed by Prof. Takakiyo Nakazawa and Shuhji Aoki (Tohoku University) for Sanriku, Japan (39.17°N, 141.83°E) for 28 August 2000, 30 May 2001, 4 September 2002, 6 September 2004, 3 June 2006, and 4 June 2007, following the procedures described by Nakazawa et al. (2002). The vertical profiles were determined by averaging the modelled and observed concentrations taken for the same day and time. The error bars show the standard deviation. To calculate the mean profiles, we subtracted the annual growth rate of 0.23 pptv/yr (Stiller et al., 2008) for SF_6 and variable growth rates derived by Conway and Tans (2011) for CO_2 for the period 2001–2007. No correction is applied to the CH_4 concentration, because a slowdown in the CH_4 increase was observed in the stratosphere for the period 1978–2003 (Rohs et al., 2006).

In general, the NIES TM is able to capture the shape of a tracer's vertical profile in the stratosphere. These profiles consist of several parts with different properties, such as: 1) weak gradients up to 70 hPa; 2) a large decrease of VMRs at heights between 70 and 50 hPa; 3) almost constant

concentrations from 50 to 30 hPa, and 4) significant (especially for CH_4) gradients from 30 hPa upwards (Figure 4).

The modelled profile of SF_6 is consistent with the observed profile up to 50 hPa and has a relatively large (~5%) positive bias above this level (Figure 4a). SF_6 is a chemically inert tracer (in the troposphere and stratosphere), indicating that transport alone is responsible for the variation in its profile. The discrepancy between the observed and simulated vertical profiles is consistent with the underestimation of the age of air above 40 hPa in temperate and high-latitude zones, as discussed above.

In contrast, the CH_4 profile was found to have a strong negative bias (~5%) between 100 and 20 hPa (Figure 4b), which disappeared with height. It would appear that a change in the CH_4 loss rate due to chemical reactions leads to a less excessive destruction of methane and a better agreement with observations above 20 hPa. SF_6 is not involved in any chemical reactions to compensate for the extra vertical transport in the UTLS region.

The simulated CO_2 vertical profile (Figure 4c) overestimated the observed profile by 0.5% below 90 hPa and underestimated it by 0.5% above 90 hPa. The individual profiles used to derive the average profile were obtained at the beginning and end of the vegetation season; consequently, the modelled CO_2 profile could show a seasonal variation at the 140–100 hPa level. The large error bars become smaller with height, enabling an estimate of the seasonal variation of approximately 1–2 ppmv at 140 hPa. The spread of data in the profiles at about 1.5 ppmv at all levels is common for measured CO_2.

Thus, the simulated vertical profiles of CH_4 and SF_6 are generally within ~5% of the observed VMRs, while CO_2 profiles are within 1%. Given that the stratosphere only represents 15%–20% of the mid-latitude atmospheric column mass, these results are sufficient for this study. It is noted that the simulated CO_2 profiles have a smoother shape and show a better consistency with the observations, as the simulation was run for 9 years less than that for CH_4 and SF_6. This result indicates the ability of the model to reproduce vertical profiles of the tracers in the lower stratosphere more accurately for a relatively short-term period (about 10 years) than for a long-term period (about 20 years). This result reflects the fact that the model tends to overestimate tracer concentrations in the uppermost part of the domain, due to sparse grid layers in the LS.

3.3. Validation of CO_2, CH_4, and SF_6 concentrations in the free troposphere

The ability of the NIES TM to simulate SF_6 and CO_2 in the near-surface layer and in the free

troposphere was validated by Belikov et al. (2011) and Niwa at al. (2011). The inter-hemispherical gradients of SF_6 and CO_2, and vertical profiles and seasonal variations of CO_2 were evaluated against the GLOBALVIEW-CO2 and World Data Centre for Greenhouse Gases (WDCGG) observations, and against an aircraft measurement dataset of CONTRAIL (Niwa at al., 2011). Although the NIES TM's performance in terms of transport, emission distribution and chemical loss, inter-hemispheric gradient, seasonal cycle, and synoptic variations in CH_4 was also quantified as part of the TransCom-CH_4 experiment (Patra et al., 2011), this section focuses on near-surface seasonal variations and vertical profiles of methane.

3.3.1. Validation of near-surface CH_4 concentrations

Given that one of the aims of this paper is to validate the modelled column-averaged concentration against ground-based FTS TCCON observations, we examined the variability of CH_4 concentrations at TCCON sites. We selected GLOBALVIEW-CH4 (GV-CH_4) sites located near to TCCON stations and the following three sites additionally: Alert (82.45°N, 62.52°W), Mauna Loa (19.53°N, 155.58°W), and Syowa (69.00°S, 39.58°E) (Table 2). Time-series plots of the modeled near-surface CH_4 concentrations were compared with *in situ* observation data. For simplicity, we refer to the names of nearby TCCON stations with surface GV-CH_4 station data. Figure 5 shows time series of the CH_4 seasonal cycle for 1990–2008, which was manually adjusted by the annual mean concentration at the South Pole.

The simulations indicate that the model underestimated the near-surface seasonal cycle at northern high-latitudes. The model bias for Alert was 13.0 ppb versus 8.4 and 6.5 ppb for Mauna Loa and Syowa, respectively. A similar feature was observed for the trend of CH_4, for which the model bias decreased from the North Pole (0.5 ppb/yr) to the South Pole (0.1 ppb/yr) (Figure 6).

Southern Australia and New Zealand are relatively isolated from large-scale CH_4 emission sources, and as a result there was some consistency between the modelled and measured values (r = 0.87–0.9 for Baring Head and Cape Grim) in capturing the small variability (amplitude of 30 ppb). As Darwin is located relatively close to the Asia tropical area (Malaysia and Indonesia), which is marked by very high variations in CH_4 emissions and complicated meteorological conditions, the model was not able to reproduce the seasonal cycle as well at this site, compared with other sites.

The results for North America, whilst including a range of emission sources, indicated a similar agreement in the phase for Park Falls and Southern Great Plains (Lamont) ($r \sim 0.7$) and performed poorly in reproducing the growth rate, as the model underestimated the trends for both sites (Figure 6).

Mixed results were also found for the European sites: good agreement with observations was found for Pic Du Midi (Orleans) and Ocean Station M (Bremen), but poor agreement for Hohenpiessenberg (Garmisch) and Pallas-Sammaltunturi (Sodankylä). However, the worst agreement in the growth rate was found for Ryori (Tsukuba), where the model systematically underestimated the seasonal variations of the tracer.

We found the very different model performance at the remote sites such as Ocean Station M (Bremen), Izaña, Cape Grim (Wollongong), Baring Head (Lauder), Alert, Mauna Loa, and Syowa, where the model was generally able to accurately reproduce the phase of variations in surface concentrations (correlation coefficients of 0.85–0.95). For other sites (Park Falls, Pallas-Sammaltunturi (Sodankylä), Ryori (Tsukuba), and Southern Great Plains (Lamont),), however, where multiple emission sources are located close by and where local meteorology plays a major role, the model encountered difficulties in reproducing the complicated CH_4 surface concentrations.

3.3.2. Validation of CH_4 vertical profiles in the troposphere

To examine the variability of CH_4 in the near-surface layer and in the free troposphere, the VMRs simulated by the model were compared against aircraft observations performed by T. Machida (NIES) in 1993–2007 over Surgut, West Siberia. This location is marked by high CH_4 emissions from wetlands.

It is challenging to perform simulations of CH_4 in the northern high-latitude regions because of large uncertainties in emissions due to under-sampling of CH_4 concentrations over most regions, particularly where melting permafrost releases CH_4 (Zhuang et al., 2009). Despite this problem, the modelled and measured values are in good agreement above 1 km (Figure 8). The model is less effective in reproducing the high variability in CH_4 concentrations in the near-surface layer and could not accurately simulate short-term variations. The VMR at the 1-km level and below was highly variable due to changes in the PBL height, which determined the volume of air absorbing all emitted tracers and the local meteorology. The greatest amount of variability was found in July and August (Figure 8), reflecting variations in the PBL height during the daytime and high emissions from wetlands.

The averaged trends derived from the biases for the levels at 1, 3, and 7 km show similar values in all cases, in the range of 40-0 ppb depending on the season. This result indicates balanced transport from the surface layer to the free troposphere due to the implementation of the JR-25/JCDAS meteorological data provided on the sigma–pressure levels.

The correlation coefficients between simulated and observed CH_4 values show an increase towards the free troposphere, from 0.19 for the 1-km level to 0.53 for the 7-km level, because vertical propagation decreases with height. While other factors are involved, changes in PBL height and associated variation in the rates of tracer redistribution from local sources to the free troposphere are important drivers of high variability in CH_4 VMR at GV-CH_4 sites with high emissions. Similar trends were obtained by Houweling et al. (2010) for four different transport models used to simulate XCO_2.

3.4. Validation of CO_2 and CH_4 column-averaged DMFs

The main goal of this paper was to validate the model's ability to reproduce the CO_2 and CH_4 column-averaged dry-air mole fractions using observations from TCCON sites, which is a global network of ground-based high-resolution FTS recording direct solar spectra in the near-infrared spectral region (Wunch et al., 2011). The overall objectives of TCCON include improving our understanding of the carbon cycle and validating XCO_2 and XCH_4 retrieved from satellite observations.

For comparison, we selected simulated and TCCON measured concentrations of XCO_2 and XCH_4 taken at around 13:00 ± 1 hour local time over TCCON sites for the period January 2009 to January 2011. Samples within this time-frame were collected for analysis, to assess the model's performance within the GOSAT overpass interval. The following the TCCON sites were selected: Bialystok (Poland, 53.22°N, 23.13°E); Bremen (Germany, 53.10°N, 8.85°E); Darwin (Australia, 12.42°S, 130.89°E); Garmisch (Germany, 47.48°N, 11.06°E); Izaña (Spain, 28.30°N, 16.50°W); Lamont (USA, 36.6°N, 97.49°W); Lauder (New Zealand, 45.04°S, 169.68°E); Orleans (France, 47.97°N, 2.11°E); Park Falls (USA, 45.95°N, 90.27°W); Sodankylä (Finland, 67.37°N, 26.63°E); Tsukuba (Japan, 36.05°N, 140.12°E); and Wollongong (Australia, 34.41°S, 150.88°E). For the Lauder site we used data from the 125HR spectrometer when available (February 2010-present) and data from the older 120HR spectrometer prior to February 2010.

To compare the modelled total column with measurements directly, it is necessary to consider the measurement averaging kernels. Averaging kernels describe the sensitivity of the retrieved total column to a perturbation in absorber abundance in a given layer of the vertical profile (Rodgers and Connor, 2003; Wunch et al., 2011). At present TCCON provides a single set of averaging kernels for CO_2 and CH_4, tabulated as a function of solar zenith angle (SZA), based on a subset of retrievals from the Lamont site (https://tccon-wiki.caltech.edu/Sites/Lamont/Averaging_Kernels). Site-specific a priori profiles used in TCCON CO_2 retrievals were provided by each site PI (https://tccon-wiki.caltech.edu/Network_Policy/Data_Use_Policy/Auxiliary_Data). A single CH_4 a priori

(independent of location and time) has been used in TCCON retrievals at all sites other than Darwin and Sodankyla. At these sites site-spicific and time-independent CH4 profiles are provided. The tabulated averaging kernels were interpolated to the SZA of the measurements and applied in the calculation of the CO_2 or CH_4 vertical column in accordance with Equation 15 of Connor et al. (2008). The tracer vertical column abundances were then divided by the dry-air column abundance to calculate the column-averaged dry air mole fractions, denoted Xy or DMF hereafter.

Due to the SZA dependence of the TCCON averaging kernels, the difference between total column concentrations calculated with and without averaging kernels is greatest for sites located farthest from the equator, Bialystok, Bremen and Sodankylä, which yield values in the range –0.6 to 2.0 ppm and –20 to 20 ppb for XCO_2 and XCH_4, respectively; the difference is smallest for the tropical and subtropical sites Darwin and Izaña, with values of –0.4 to 0.4 ppm and –5.0 to 5.0 ppb, respectively.

Time series of the model results and FTS data for XCO_2 and XCH_4 are shown in Figures 10 and 12, respectively. These figures were produced by manually adjusting the XCO_2 and XCH_4 model offsets (2.2 ppm and –32.0 ppb, respectively). The offsets were caused by the use of slightly out-dated fluxes for the simulations, the implementation of an averaging kernel, and misfit in the modelled vertical profiles. Thus, XCH_4 may be affected due to high uncertainty of OH, which is responsible for CH_4 destruction in the atmosphere.

Matching the model's mean CH_4 with the observations is achieved by adjusting either global total emissions or sinks, which both have large uncertainties (10-20%, Patra et al, 2011). Small residual offsets can be adjusted by tuning global emissions, but long-term simulations are required to reach and equilibration between sources and sinks. Adding a small 30 ppb offset to simulated results is nearly equivalent to the corresponding proportional change in the emissions fields on the order of 2%. For CO_2, the corresponding bias correction is about 0.5%.

For TCCON, the observation symbols and error bars represent the mean and standard deviations of the weighted average if more than one measurement within the 13:00 ± 1 hour local time was available. Note that gaps in the TCCON data time-series are due to cloud and instrumental issues.

3.4.1. Modelled XCH_4 compared with TCCON FTS observations

Reproducing the CH_4 seasonal variation was a big challenge, because of its rather small amplitude and high scatter relative to the mean climatological value. As expected, the seasonal

variation in XCH_4 over the Southern Hemisphere (i.e., Darwin, Lauder, and Wollongong) was weak (Figure 10a, g, h) due to the smaller contribution of the local emissions; consequently, the model ability to reproduce the variation generally depends on reproducing of large-scale transport. The correlation coefficients for these sites are very similar (0.55, 0.58, and 0.66, respectively; Table 3).

In contrast, model performance at the Northern sites is strongly depends on powerful local sources. The best correlation coefficients (in the range of 0.62-0.74) are obtained for Lamont, Bremen and Bialystok, where seasonal variation in XCH_4 has a highest amplitude among considered sites. European sites show slightly large biases of 4.52, -8.80, and 20.91 for Bialystok, Orleans and Sodankylä, respectively. For Orleans the correlation is rather weak (0.59, Table 3), whereas for the corresponding GlobalView station of Pic Du Midi it is rather strong (>0.85, Fig. 7). This is due to the fact that Pic Du Midi is a high altitude site (free troposphere) and Orleans a lowland site affected by surface-near small scale processes. For Sodankylä the modelled time-series profile has two-peak shape representing two maximum of the concentration. One maximum is due to anthropogenic influence in the end of winter and beginning of spring, another is caused by wetland emissions in the beginning of fall. However, FTS measurements are not able to capture spring maximum, and as a result, there is a large bias (b=20.91 ppb) and low correlation coefficient (r = 0.40) for this site.

For Wollongong, the simulated results were strongly underestimated (bias -11.05ppb), as the FTSs amplitude of seasonal variation was found to be twice (Figure 10*l*) the model value and twice that for other TCCON sites in the Southern Hemisphere. The reasons for this result remain unclear, although it may be relevant that Wollongong is located near major urban centres and sites of industrial activity, where emissions from coal mining are the largest source above background (Fraser et al., 2011).

Izaña is oceanic site located on a small island. The model's grid is too rough to reproduce local emission and loss. The model is not able to reproduce small-scale variation of concentration, as results, weak correlation (0.53) and large bias (9.05 ppb).

In general, the minimum and maximum bias between the two datasets is –8.80 ppb (–0.49 %) and 20.91 ppb (1.16 %), respectively. Figure 11 shows a scatter diagram of model XCH_4 data versus ground-based FTS XCH_4 data for 12 sites. The majority of points are within an interval of ±1% of XCH_4

3.4.2. Modelled XCO_2 compared with TCCON FTS observations and GECM

We compared XCO_2 time-series with TCCON and constructed a 3-D CO_2 climatology GECM (Gap-filled and Ensemble Climatology Mean) (Saito et al., 2011) (Figure 12). The seasonally varying climatology in GECM was estimated by taking an ensemble of the various transport models in combination with the interpolated bias correction, using a data product based on *in situ* measurements in the troposphere (GLOBALVIEW-CO2, 2010) and the monthly vertical and latitudinal distribution of the ACTM-derived mean age of air in the stratosphere. Six transport models (ACTM, LMDZ4, NICAM, PCTM, and TM5), including the previous version of NIES TM (Belikov et al., 2011), participated in this study, but this is considered unlikely to seriously distort the results. The GECM seasonal cycle was nudged towards a seasonal cycle of the extended CO_2 record (GLOBALVIEW-CO2, 2010) by filtering out the inter-annual anomalies and the synoptic variability in the extended CO_2 records using a curve-fitting procedure (Masarie and Tans, 1995).

The modelled XCO_2 and GECM XCO_2 time series show strong correlations with the TCCON data (correlation coefficients of 0.8–0.9; Table 3), as the seasonal XCO_2 variation is stronger than the XCH_4 cycle. Because of the use of actual meteorology and more up-to-date fluxes, the NIES TM described the seasonal variations slightly better for Bialystok, Bremen, Darwin, Lamont, Lauder, and Wollongong. Moreover, for all sites except Park Falls, Tsukuba, and Wollongong, the model bias was less than the bias for GECM. At other sites, comparisons of the model versus FTS and GECM versus FTS produced almost identical results.

The model shows quite good results in reproducing different seasonal cycles for all considered sites, including very steep decreasing of XCO_2 at Sodankylä during vegetation period and almost flat profiles at sites in the Southern Hemisphere. Figure 13 shows a scatter diagram of model XCO_2 data versus ground-based FTS XCO_2 data. The minimum and maximum differences in the model data compared with the FTS data are -0.62 ppm (-0.16 %) and 1.21 ppm (0.31 %), respectively.

For XCO_2 there are several events with only one FTS measurement taken at approximately 13:00 ± 1 hour local time. Generally, the standard error in such cases is quite large especially for Lamont and Tsukuba (Figure 12f, k).

4. Discussion

The model was able to reproduce the seasonal and inter-annual variability of XCO_2 and XCH_4 with correlation coefficients of 0.8–0.9 and 0.4–0.7, respectively. A small correlation was obtained for methane, due to the weak seasonal cycle of CH_4 and a high scatter of XCH_4 obtained from the ground FTS data within the selected interval (13:00 ± 1 hour local time). The modeled time-series have quite small biases for all sites excluding Sodankylä, where model show large bias both for XCO_2 and XCH_4, 1.21 ppm and 20.91 ppb, respectively. Moreover, GECM results also has large misfit (1.22 ppm) for this site. Without Sodankylä's data bias of modeled results is ±0.2% and ±0.5% for XCO_2 and XCH_4, respectively.

In contrast to CO_2, the modeled vertical profiles of CH_4 show large deviations from the limited set of a priori profiles used in TCCON CH_4 retrievals to date. If true atmospheric vertical structure and variability in tracer mixing ratios are not adequately represented in the TCCON retrieval a priori, retrieval errors may result. TCCON retrieval a priori profiles for non-CO_2 gases have been substantially improved in the upcoming revision of the TCCON retrieval algorithm. It will be of interest to repeat the model intercomparison with TCCON XCH_4 once the TCCON data have been reanalysed.

The tracer column-averaged dry-air mole fraction is a sensitive indicator of overall model performance, because it is relatively unaffected by changes in vertical transport and surface pressure, and shows minor spatial and temporal variations. As a result, the total column represents the model performance on a global scale. The XCO_2 and especially the XCH_4 scatter diagrams (Figures 11 and 13, respectively) show balanced redistributions of tracer concentrations from the Northern Hemisphere, with high emissions to the Southern Hemisphere reproduced by the model. Moreover, the Darwin site shows vertical redistribution due to powerful tracer outflow from the PBL into the troposphere and the stratosphere, because this site is located in the tropics. The good agreement between simulated XCH_4 and FTS measurements highlights the ability of the model to capture the vertical profile of tracers, and in particular, to simulate balanced transport across the tropopause, as the mean age of methane was markedly different in the lower stratosphere and upper troposphere.

5. Conclusion

We performed multi-annual simulations of CO_2, CH_4, and SF_6 using the NIES three-dimensional offline chemical transport model (version NIES-08.1i), driven by JRA-25/JCDAS reanalysis data. This version uses a flexible hybrid sigma–isentropic (σ–θ) vertical coordinate consisting of terrain-following and isentropic levels switched smoothly near the tropopause. Vertical transport in the isentropic part of the grid in the stratosphere was controlled by an air-ascending rate derived from the effective heating rate from JRA-25/JCDAS reanalysis, and was adjusted to fit the observed age of air in the stratosphere. The use of this vertical transport scheme avoided spurious vertical mixing caused by interpolation of the meteorological vertical wind component, and this resulted in improved model performance in the stratosphere, as the simulated vertical profiles of CO_2, CH_4, and SF_6 showed good agreement with balloon-borne observations. A comparison of model data with balloon-borne observations over Sanriku (Japan) in 2000–2007 revealed that the tracer transport simulations were performed with accuracies of ~5% for CH_4 and SF_6, and ~1% for CO_2 compared with the observed VMRs.

We evaluated the model performance in simulating near-surface CH_4 concentrations by comparisons with measurements at GLOBALVIEW-CH4 sites. In general, the model was able to reproduce the variations in the surface concentrations more accurately ($r = 0.6–0.8$) at sites located some distance away from multiple emission sources. For other sites, where high emissions and local meteorology play a major role, it proved difficult to reproduce the CH_4 surface concentrations.

For measurements above 1 km, the model data are in good agreement with aircraft observations (1993–2007) over Surgut, West Siberia, which is an area with high emissions of methane from wetlands. However, the model was less effective in reproducing the high variability of CH_4 concentrations in the near-surface layer and did not simulate short-term variations with any reasonable accuracy. These results are in agreement with the findings of Houweling et al. (2010), and highlight the importance of obtaining a realistic representation of PBL dynamics, especially in regions with high tracer emissions.

Convolved with scene-dependent instrument averaging kernels, XCO_2 and XCH_4 were calculated from NIES TM tracer distributions and were compared with measurements acquired at TCCON ground-based FTS sites for the period from January 2009 to January 2011. The model was able to reproduce the seasonal and inter-annual variability of XCO_2 and XCH_4 with correlation coefficients of 0.8–0.9 and 0.4–0.8, respectively. A comparison of modelled data and TCCON observations revealed that the model biases are ±0.2% for XCO_2 and ±0.5% for XCH_4 without Sodankylä's data.

In general, the overall performance of NIES TM at TCCON sites is similar to the performance of four transport models (IFS, LMDZ, TM3, and TM5) compared by Houweling et al. (2010) for XCO_2 and to GEOS-Chem TM results published by Parker et al. (2011) for XCH_4. Although the focus of future work will be to further improve and validate XCO_2 and XCH_4 simulations, the performance of the current model version is sufficient for use in evaluating satellite retrieval algorithms in areas not covered by ground-based FTS sites.

Acknowledgments

We thank T. Machida for aircraft observations of CH_4 over Surgut (Russia); and A.E. Andrews, T.M. Hall, and D.W. Waugh for providing observation data of the mean age of air in the stratosphere. We also thank P.K. Patra and the TransCom-CH_4 and CONTRAIL TMI communities for model setups, initial profiles, and emission fluxes used in the tracer transport simulation. We also thank S. Oshchepkov for insightful discussions and suggestions regarding the manuscript. The meteorological datasets used for this study were provided by the cooperative research project of the JRA-25/JCDAS long-term reanalysis by the Japan Meteorological Agency (JMA) and the Central Research Institute of Electric Power Industry (CRIEPI). We also thank GLOBALVIEW-CO_2/CH_4 authors. For calculations, we used the computational resources of the NIES supercomputer system (NEC SX-8R/128M16).

TCCON data were obtained from the TCCON Data Archive, operated by the California Institute of Technology from the website at http://tccon.ipac.caltech.edu/. US funding for TCCON comes from NASA's Terrestrial Ecology Program, grant number NNX11AG01G, the Orbiting Carbon Observatory Program, the Atmospheric CO_2 Observations from Space (ACOS) Program and the DOE/ARM Program. The Darwin TCCON site was built at Caltech with funding from the OCO project, and is operated by the University of Wollongong, with travel funds for maintenance and equipment costs funded by the OCO-2 project. We acknowledge funding to support Darwin and Wollongong from the Australian Research Council, Projects LE0669470, DP0879468, DP110103118 amd LP0562346. Lauder TCCON measurements are funded by New Zealand Foundation of Research Science and Technology contracts C01X0204 and CO1X0406. We acknowledge financial support of the Bialystok and Orleans TCCON sites from the Senate of Bremen and EU projects IMECC and GEOmon, as well as maintenance and logistical work provided by AeroMeteo Service (Bialystok) and the RAMCES team at LSCE (Gif-sur-Yvette, France) and additional operational funding from the National Institute for Environmental Studies (NIES, Japan).

Reference

1. Andrews, A. E., Boering, K. A., Daube, B. C., Wofsy, S. C., Loewenstein, M., Jost, H., Podolske, J. R., Webster, C. R., Herman, R. L., Scott, D. C., Flesch, G. J., Moyer, E. J., Elkins, J. W., Dutton, G. S., Hurst, D. F., Moore, F. L., Ray, E. A., Romashkin, P. A., and Strahan, S. E.: Mean ages of stratospheric air derived from in situ observations of CO_2, CH_4, and N_2O, Journal of Geophysical Research, 106, 32295–32314, doi:10.1029/2001JD000465, http://www.agu.org/pubs/crossref/2001/2001JD000465.shtml, 2001.

2. Arakawa, A., and Moorthi, S.: Baroclinic instability in vertically discrete systems, J. Atmos. Sci., 45, 1688–1707, 1988.

3. Austin, P.M. and Houze Jr., R.A.: A technique for computing vertical transports by precipitating cumuli, J. Atmos. Sci., 30, 1100–1111, 1973.

4. Baker, D. F., Law, R. M., Gurney, K. R., Rayner, P., Peylin, P., Denning, A. S., Bousquet, P., Bruhwiler, L., Chen, Y.-H., Ciais, P., Fung, I. Y., Heimann, M., John, J., Maki, T., Maksyutov, S., Masarie, K., Prather, M., Pak, B., Taguchi, S., and Zhu, Z.: TransCom 3 inversion intercomparison: Impact of transport model errors on the interannual variability of regional CO_2 fluxes 1988–2003, Global Biogeochem. Cycles, 20, GB1002, doi:10.1029/2004GB002439, http://dx.doi.org/10.1029/2004GB002439, 2006.

5. Belikov, D., Maksyutov, S., Miyasaka, T., Saeki, T., Zhuravlev, R., and Kiryushov, B.: Mass-conserving tracer transport modelling on a reduced latitude-longitude grid with NIES-TM, Geosci. Model Dev., 4, 207-222, 2011.

6. Bergamaschi, P., Frankenberg, C., Meirink, J.F., Krol, M., Dentener, F., Wagner, T., Platt, Y., Kaplan, J.O., Kroner, S., Heimann, M., Dlugokencky, E. J., and Goede, A.: Satellite cartography of atmospheric methane from SCIAMACHY on board ENVISAT: 2. Evaluation based on inverse model simulations, J. Geophys. Res., 112, D02304, doi:10.1029/2006JD007268, 2007.

7. Bergamaschi, P., Frankenberg, C., Meirink, J. F., Krol, M., Villani, M. G., Houweling, S., Dentener, F., Dlugokencky, E. J., Miller, J. B., Gatti, L. V., Engel, A., and Levin, I.: Inverse modeling of global and regional CH4 emissions using SCIAMACHY satellite retrievals, J. Geophys. Res., 114, D22301, doi:10.1029/2009JD012287, 2009.

8. Bloom, A.A., Palmer, P.I., Fraser, A., David, S.R., and Frankenberg C.: Large-scale controls of methanogenesis inferred from methane and gravity space-borne data, Science, 327 (5963), 322–325, doi:10.1126/science.1175176, 2010.

9. Bleck, R.: On the use of hybrid vertical coordinates in numerical weather prediction models, Mon. Wea. Rev., 106, 1233–1244, 1978.

10. Boden, T. A., Marland, G., and Andres, R. J.: Global, Regional, and National Fossil Fuel CO_2 Emissions, Carbon Dioxide Information Analysis Center, Oak Ridge National Laboratory, U.S. Department of Energy, Oak Ridge, Tenn, USA, doi:10.3334/CDIAC/00001, 2009.

11. Boering, K. A., Wofsy, S.C., Daube, B.C., Schneider, H. R., Loewenstein, M., and Podolske, J.R.: Stratospheric transport rates and mean age distribution derived from observations of atmospheric CO_2 and N_2O, Science, 274, 1340– 1343, 1996.

12. Bousquet, P., Ciais, P., Miller, J. B., Dlugokencky, E. J., Hauglustaine, D. A., Prigent, C., van der Werf, G. R., Peylin, P., Brunke, E.-G., Carouge, C., Langenfelds, R. L., Lathi ´ ere, J., Papa, F., Ramonet, M., Schmidt, M., Steele, L. P., Tyler, S. C., and White, J.: Contribution of anthropogenic and natural sources to atmospheric methane variability, Nature, 443, 439–443, doi:10.1038/nature05132, 2006.

13. Butz, A., Guerlet, S., Hasekamp, O., Schepers, D., Galli, A., Aben, I., Frankenberg, C., Hartmann, J. -M., Tran, H., Kuze, A., Keppel-Aleks, G., Toon, G., Wunch, D., Wennberg, P., Deutscher, N., Griffith, D., Messerschmidt, J., Macatangay, R., Notholt, J., Warneke, T.: Toward accurate CO_2 and CH_4 observations from GOSAT, Geophys. Res. Lett., 38, L14812, doi:10.1029/2011GL047888, 2011.

14. Bovensmann, H., Burrows, J.P., Buchwitz, M., Frerick, J., Noël, S., Rozanov, V.V., Chance, K.V., and Goede, A.H.P.: SCIAMACHY - Mission objectives and measurement modes, J. Atmos. Sci., 56, (2), 127-150, 1999.

15. Chipperfield, M.P.: New Version of the TOMCAT/SLIMCAT Off-Line Chemical Transport Model: Intercomparison of Stratospheric Tracer Experiments, Q. J. R. Meteorol. Soc., 132, 1179-1203, doi:10.1256/qj.05.51, 2006.

16. Conway, T. J., Tans, P.P., Waterman, L.S., Thoning, K.W., Kitzis, D.R., Masarie, K.A., and Zhang N.: Evidence for interannual variability of the carbon cycle from the National Oceanic and Atmospheric Administration/Climate Monitoring and Diagnostics Laboratory Global Air Sampling Network, J. Geophys. Res., 99(D11), 22,831–22,855, doi:10.1029/94JD01951, 1994.

17. Conway T. and P. Tans, NOAA/ESRL (www.esrl.noaa.gov/gmd/ccgg/trends/)

18. Douglass, A.R., Prather, M.J., Hall, T.M., Strahan, S.E., Rasch, P.J., Sparling, L.C., Coy, L., and Rodriguez J.M.: Choosing meteorological input for the global modeling initiative assessment of high-speed aircraft, J. Geophys. Res., 104, 27,545– 27,564, 1999.

19. Denning, A.S., Randall, D.A., Collatz, G.J., and Sellers, P.J.: Simulations of terrestrial carbon metabolism and atmospheric CO_2 in a general circulation model. II. Simulated CO_2 concentrations, Tellus B Chem. Phys. Meteorol., 48, 543–567, doi:10.1034/j.1600-0889. 1996.t01-1-00010.x, 1996

20. Eguchi, N., Saito, R., Saeki, T., Nakatsuka, Y., Belikov, D., and Maksyutov S.: A priori covariance estimation for CO_2 and CH_4 retrievals, J. Geophys. Res., 115, D10215, doi:10.1029/2009JD013269, 2010.

21. Eliassen, A., and Raustein, E.: A numerical integration experiment with a model atmosphere based on isentropic coordinates, Meteorologiske Annaler, 5, 45-63, 1968.

22. Elkins, J. W., Fahey, D. W., Gilligan, J. M., Dutton, G. S., Baring, T. J., Volk, C. M., Dunn, R.

E., Myers, R. C., Montzka, S. A., Wamsley, P. R., Hayden, A. H., Butler, J. H., Thompson, T. M., Swanson, T. H., Dlugokencky, E. J., Novelli, P. C., Hurst, D. F., Lobert, J. M., Ciciora, S. J., McLaughlin, R. J., Thompson, T. L., Winkler, R. H., Fraser, P. J., Steele, L. P., and Lucarelli, M. P.: Airborne gas chromatograph for in situ measurements of long lived species in the upper troposphere and lower stratosphere,Geophys. Res. Lett., 23, 347–350, 1996

23. Eluszkiewicz, J., Helmer, R.S., Mahlman, J.D., Bruhwiler, L. and Takacs, L.L.: Sensitivity of age-of-air calculations to the choice of advection scheme, J. Atmos. Sci., 57, 3185-3201, 2000.

24. Engel, A., Möbius, T., Bönisch, H., Schmidt, U., Heinz, R., Levin, I., Atlas, E., Aoki, S., Nakazawa, T., Sugawara, S., Moore, F., Hurst, D., Elkins, J., Schauffler, S., Andrews, A., Boering, K.: Age of stratospheric air unchanged within uncertainties over the past 30 years, Nature Geoscience, 2, 28-31, doi:10.1038/ngeo388, 2009.

25. Feichter, J., and Crutzen, P.J.: Parameterization of vertical transport due to deep cumulus convection in a global transport model and its evaluation with ^{222}Rn measurements, Tellus B, 42, 100–117, 1990.

26. Folkins, I., Loewenstein, M., Podolske, J., Oltmans, S.J., and Proffitt M.: A barrier to vertical mixing at 14 km in the tropics: Evidence from ozone sondes and aircraft measurements, J. Geophys. Res., 104(D18), 22, 095–22, 102, 1999.

27. Fraser, A., Chan Miller, C., Palmer, P.I., Deutscher, N.M., Jones, N.B., and Griffith D.W.T.: The Australian methane budget: Interpreting surface and train ‐ borne measurements using a chemistry transport model, J. Geophys. Res., 116, D20306, doi:10.1029/2011JD015964, 2011.

28. Fueglistaler, S., Legras, B., Beljaars, A., Morcrette, J. J., Simmons, A., Tompkins, A. M., Uppala, S.: The diabatic heat budget of the upper troposphere and lower/mid stratosphere in ECMWF reanalysis, Q. J. Roy. Meteor. Soc., 135(638), 21–37, 2009.

29. Gettelman, A., de F. Fujiwara, P.M., Fu, Q., Voemel, H., Gohar, L.K., Johanson, C., and Ammeraman, M.: Radiation balance of the tropical tropopause layer, J. Geophys. Res., 109, D07103, doi:10.1029/2003JD004190, 2004.

30. GLOBALVIEW-CH4 (2009), Cooperative Atmospheric Data Integration Project – Methane. CD-ROM, NOAA ESRL, Boulder, Colorado [Also available on Internet via anonymous FTP to ftp.cmdl.noaa.gov, Path: ccg/ch4/GLOBALVIEW].

31. GLOBALVIEW-CO2 (2010), Cooperative Atmospheric Data Integration Project – Carbon Dioxide. CD-ROM, NOAA ESRL, Boulder, Colorado [Also available on Internet via anonymous FTP to ftp.cmdl.noaa.gov, Path: ccg/co2/GLOBALVIEW].

32. Grell, G. A.: Prognostic evaluation of assumptions used by cumulus parameterizations, Mon. Weather Rev., 121, 764–787, 1993.

33. Gurney, K. R., Law, R.M., Denning, A.S., Rayner, P.J., Pak, B.C., Baker, D., Bousquet, P., Bruhwiler, L., Chen, Y.H., Ciais, P., Fung, I.Y., Heimann, M., John, J., Maki, T., Maksyutov, S., Peylin, P., Prather, M., and Taguchi, S.: Transcom 3 inversion intercomparison: Model mean

744 results for the estimation of seasonal carbon sources and sinks, Global Biogeochem. Cy., 18,
745 GB1010, doi:10.1029/2003GB002111,2004.

746 34. Hack, J.J., Boville, B.A., Briegleb, B.P., Kiehl, J.T., Rasch, P.J., and Williamson, D.L.:
747 Description of the NCAR community climate model (CCM2), NCAR/TN-382, 108, 1993.

748 35. Hall, T.M., Waugh, D.W., Boering, K.A., and Plumb R.A.: Evaluation of transport in
749 stratospheric models, J. Geophys. Res., 104(D15), 18815–18839, 1999.

750 36. Harnisch, J., Borchers, R., Fabian, P., and Maiss M.: CF_4 and the Age of Mesospheric and Polar
751 Vortex Air, Geophys. Res. Lett., 26(3), 295-298, 1999.

752 37. Houweling, S., Aben, I., Breon, F.-M., Chevallier, F., Deutscher, N., Engelen, R., Gerbig, C.,
753 Griffith, D., Hungershoefer, K., Macatangay, R., Marshall, J., Notholt, J., Peters, W., and Serrar,
754 S.: The importance of transport model uncertainties for the estimation of CO_2 sources and sinks
755 using satellite measurements, Atmos. Chem. Phys., 10, 9981-9992, doi:10.5194/acp-10-9981-
756 2010, 2010.

757 38. Hsu, Y.-J. G., and Arakawa, A.: Numerical modeling of the atmosphere with an isentropic
758 vertical coordinate, Mon. Wea. Rev., 118, 1933–1959, 1990.

759 39. Ingmann, P.: A-SCOPE, Advanced space carbon and climate observation of planet earth, Report
760 for Assessment, SP-1313/1, ESA communication production office, Noordwijk, The Netherlands,
761 2009.

762 40. Intergovernmental Panel on Climate Change (IPCC), Climate change 2007: The Physical Science
763 Basis: Contribution of Working Group I to the Fourth Assessment Report of the
764 Intergovernmental Panel on Climate Change, edited by: Solomon, S., Qin, D., Manning, M.,
765 Chen, Z., Marquis, M., Averyt, K. B., Tignor, M., and Miller, H. L., Cambridge University Press,
766 Cambridge, UK and New York, NY, USA, 996 pp., 2007.

767 41. Kalnay E.: Atmospheric Modeling, Data Assimilation and Predictability, Cambridge University
768 Press, 364 (ISBN-10: 0521796296, ISBN-13: 978-0521796293), 2002.

769 42. Keppel-Aleks, G., Wennberg, P. O. and Schneider, T.: Sources of variations in total column
770 carbon dioxide, Atmos. Chem. Phys. 11, 3581–3593, 2011.

771 43. Konopka, P., Günther, G., Müller, R., dos Santos, F.H.S., Schiller, C., Ravegnani, F., Ulanovsky,
772 A., Schlager, H., Volk, C.M., Viciani, S., Pan, L.L., McKenna, D.-S., and Riese, M.:
773 Contribution of mixing to upward transport across the tropical tropopause layer (TTL), Atmos.
774 Chem. Phys., 7, 3285–3308, http://www.atmos-chem-phys.net/7/3285/2007/, 2007.

775 44. Konor, C. S., and Arakawa, A.: Design of an atmospheric model based on a generalized vertical
776 coordinate, Mon. Weather Rev., 125, 1649 – 1673, 1997.

777 45. Levin, I., Naegler, T., Heinz, R., Osusko, D., Cuevas, E., Engel, A., Ilmberger, J., Langenfelds,
778 R.L., Neininger, B., Rohden, C.V., Steele, L.P., Weller, R., Worthy, D.E., and Zimov, S.A.: The
779 global SF_6 source inferred from long-term high precision atmospheric measurements and its

780 comparison with emission inventories, Atmos. Chem. Phys., 10, 2655–2662, doi:10.5194/acp-10-
781 2655-2010, 2010.

782 46. Mahowald, N.M., Plumb, R.A., Rasch, P.J., del Corral, J., and Sassi, F.: Stratospheric transport in
783 a three-dimensional isentropic coordinate model, J. Geophys. Res., 107(D15), 4254,
784 doi:10.1029/2001JD001313, 2002.

785 47. Maiss, M., Steele, L.P., Francey, R.J., Fraser, P.J., Langenfelds, R.L., Trivett N.B.A. and Levin
786 I.: Sulfur hexafluoride – a powerful new atmospheric tracer, Atmos. Environ., 30, 1621-1629,
787 1996.

788 48. Maksyutov, S., Patra, P.K., Onishi, R., Saeki, T., and Nakazawa, T.: NIES/FRCGC global
789 atmospheric tracer transport model: description, validation, and surface sources and sinks
790 inversion, J. Earth Simulator, 9, 3–18, 2008.

791 49. Masarie, K.A. and Tans P. P.: Extension and integration of atmospheric carbon dioxide data into
792 a globally consistent measurement record, J. Geophys. Res., 100, 11593–11610, 1995.

793 50. Meirink J.-F., Eskes, H.J., and Goede, A.P.H.: Sensitivity analysis of methane emissions derived
794 from SCIAMACHY observations through inverse modeling, Atmos. Chem. Phys. 6, 1275–1292,
795 2006.

796 51. Miyazaki, K., Patra, P. K., Takigawa, M., Iwasaki, T., and Nakazawa, T.: Global-scale transport
797 of carbon dioxide in the troposphere, J. Geophys. Res., 113, D15301,
798 doi:10.1029/2007JD009557, 2008.

799 52. Monge-Sanz, B.M., Chipperfield, M.P., Simmons, A. J., and Uppala S. M.: Mean age of air and
800 transport in a CTM: Comparison of different ECMWF analyses, Geophys. Res. Lett., 34,
801 L04801, doi:10.1029/2006GL028515, 2007.

802 53. Morino, I., Uchino, O., Inoue, M., Yoshida, Y., Yokota, T., Wennberg, P.O., Toon, G.C., Wunch,
803 D., Roehl, C.M., Notholt, J., Warneke, T., Messerschmidt, J., Griffith, D.W. T., Deutscher, N.M.,
804 Sherlock, V., Connor, B., Robinson, J., Sussmann, R., and Rettinger, M.: Preliminary validation
805 of column-averaged volume mixing ratios of carbon dioxide and methane retrieved from GOSAT
806 short-wavelength infrared spectra, Atmos. Meas. Tech., 4, 1061–1076, doi:10.5194/amt-4-1061-
807 2011, 2011.

808 54. Nakazawa T., Aoki, S., Kawamura, K., Saeki, T., Sugawara, S., Honda, H., Hashida, G.,
809 Morimoto, S., Yoshida, N., Toyoda, S., Makide, Y., Shirai, T.: Variations of stratospheric trace
810 gases measured using a balloon-borne cryogenic sampler, Advances in Space Research, 30, 5,
811 1349-1357, ISSN 0273-1177, DOI: 10.1016/S0273-1177(02)00551-3, 2002.

812 55. Niwa, Y., Patra, P. K., Sawa, Y., Machida, T., Matsueda, H., Belikov, D., Maki, T., Ikegami, M.,
813 Imasu, R., Maksyutov, S., Oda, T., Satoh, M., and Takigawa, M.: Three-dimensional variations
814 of a$_t$mospheric CO2: aircraft measurements and multi-transport model simulations, Atmos.
815 Chem. Phys., 11, 13359-13375, doi:10.5194/acp-11-13359-2011.

816 56. Olivier, J.G.J. and Berdowski, J.J.M.: Global emissions sources and sinks, A.A. Balkema

817 Publishers/Swets and Zeitlinger Publishers, Lisse, The Netherlands, 2001.

818 57. Onogi, K., Tsutsui, J., Koide, H., Sakamoto, M., Kobayashi, S., Hatsushika, H., Matsumoto, T.,
819 Yamazaki, N., Kamahori, H., Takahashi, K., Kadokura, S., Wada, K., Kato, K., Oyama, R., Ose,
820 T., Mannoji, N., and Taira, R.: The JRA-25 Reanalysis, J. Met. Soc. Jap., 85(3), 369-432, 2007.

821 58. Parker, R., Boesch, H., Cogan, A., Fraser, A., Feng, L., Palmer, P.I., Messerschmidt, J.,
822 Deutscher, N., Griffith, D.W.T., Notholt, J., Wennberg, P.O., and Wunch, D.: Methane
823 observations from the Greenhouse Gases Observing SATellite: Comparison to ground-based
824 TCCON data and model calculations, Geophys. Res. Lett., 38, L15807,
825 doi:10.1029/2011GL047871, 2011.

826 59. Patra, P. K., Houweling, S., Krol, M., Bousquet, P., Belikov, D., Bergmann, D., Bian, H.,
827 Cameron-Smith, P., Chipperfield, M. P., Corbin, K., Fortems-Cheiney, A., Fraser, A., Gloor, E.,
828 Hess, P., Ito, A., Kawa, S. R., Law, R. M., Loh, Z., Maksyutov, S., Meng, L., Palmer, P. I., Prinn,
829 R. G., Rigby, M., Saito, R., and Wilson, C.: TransCom model simulations of CH4and related
830 species: linking transport, surface flux and chemical loss with CH4 variability in the troposphere
831 and lower stratosphere, Atmos. Chem. Phys., 11, 12813-12837, doi:10.5194/acp-11-12813-2011,
832 2011.

833 60. Plumb, R.A. and Ko, M.K.W.: Interrelationships between mixing ratios of long-lived
834 stratospheric constituents, J.Geophys. Res., 97, 10145–10156, 1992.

835 61. Rayner, P.J. and O'Brien D.M.: The utility of remotely sensed CO_2 concentration data in surface
836 source inversions, Geophys. Res. Lett., 28, 175–178, 2001.

837 62. Ray, E.A., Moore, F.L., Elkins, J.W., Dutton, G.S., Fahey, D.W., Vömel, H., Oltmans, S.J., and
838 Rosenlof, K.H.: Transport into the Northern Hemisphere lowermost stratosphere revealed by in
839 situ tracer measurements, J. Geophys. Res., 104(D21), 26565–26580, 1999.

840 63. Rodgers, C.D., and Connor, B.J.: Intercomparison of remote sounding instruments. J. Geophys.
841 Res. 108, 4116–4229, doi:10.1029/2002JD002299, 2003.

842 64. Rohs, S., Schiller, C., Riese, M., Engel, A., Schmidt, U., Wetter, T., Levin, I., Nakazawa, T.,
843 Aoki, S.: Long-term changes of methane and hydrogen in the stratosphere in the period 1978-
844 2003, J. Geophys. Res., 111, D14315, doi:10.1029/2005JD006877, 2006.

845 65. Saito R., Houweling, S., Patra, P.K., Belikov, D., Lokupitiya, R., Niwa, Y., Chevallier, F., Saeki,
846 T., and Maksyutov S.: TransCom satellite intercomparison experiment: Construction of a bias
847 corrected atmospheric CO_2 climatology, J. Geophys. Res., 116, D21120,
848 doi:10.1029/2011JD016033, 2011.

849 66. Sherwood, S.C., and Dessler, A.E.: Convective mixing near the tropopause: Insights from
850 seasonal variations, J. Atmos. Sci., 60(22), 2674–2685, 2003.

851 67. Stiller G.P., von Clarmann, T., Hopfner, M., Glatthor, N., Grabowski, U., Kellmann, S., Kleinert,
852 A., Linden, A., Milz, M., Reddmann, T., Steck, T., Fischer, H., Funke, B., Lopez-Puertas, M.,
853 and Engel, A.: Global distribution of mean age of stratospheric air from MIPAS SF_6

854 measurements, Atmos. Chem. Phys., 8, 677–695, 2008.

855 68. Tiedtke, M.: A comprehensive mass flux scheme for cumulus parameterization in large scale
856 models, Mon. Weather Rev., 117, 1779-1800, 1989.

857 69. Thuburn, J., and Craig, G.C.: On the temperature structure of the tropical substratosphere, J.
858 Geophys. Res., 107(D2), 4017, doi:10.1029/2001JD000448, 2002.

859 70. Zhuang, Q., Melack, J.M., Zimov, S., Walter, K.M., Butenhoff, C.L., and Khalil, M.A.K., Global
860 methane emissions from wetlands, rice paddies, and lakes, Eos, 90(5), 37-38, 2009.

861 71. Washenfelder, R.A., Wennberg, P.O., and Toon, G.C.: Tropospheric methane retrieved from
862 ground-based near-IR solar absorption spectra, Geophys. Res. Lett., 30(23), 2226,
863 doi:10.1029/2003GL017969, 2003.

864 72. Waugh, D.W., and Hall, T.M.: Age of stratospheric air: Theory, observations, and models, Rev.
865 Geophys., 40 (4), 10.1029/2000RG000101, 2002.

866 73. Weaver, C.J., Douglass, A.R., and Rood, R.B.: Thermodynamic balance of three-dimensional
867 stratospheric winds derived from a data assimilation procedure, J. Atmos. Sci., 50, 2987-2993,
868 1993.

869 74. Wunch, D., Toon, G.C., Wennberg, P.O., Wofsy, S.C., Stephens, B.B., Fischer, M.L., Uchino,
870 O., Abshire, J.B., Bernath, P., Biraud, S.C., Blavier, J.-F. L., Boone, C., Bowman, K.P., Browell,
871 E.V., Campos, T., Connor, B.J., Daube, B.C., Deutscher, N.M., Diao, M., Elkins, J.W., Gerbig,
872 C., Gottlieb, E., Griffith, D.W.T., Hurst, D.F., Jimenez, R., Keppel-Aleks, G., Kort, E. A.,
873 Macatangay, R., Machida, T., Matsueda, H., Moore, F., Morino, I., Park, S., Robinson, J., Roehl,
874 C. M., Sawa, Y., Sherlock, V., Sweeney, C., Tanaka, T., and Zondlo, M. A.: Calibration of the
875 Total Carbon Column Observing Network using aircraft profile data, Atmos. Meas. Tech., 3,
876 1351–1362, doi:10.5194/amt-3-1351-2010, 2010.

877 75. Wunch, D., Toon, G., Blavier, J.-F. L., Washenfelder, R.A., Notholt, J., Connor, B.J., Griffith,
878 D.W.T., Sherlock, V., and Wennberg, P.O.: The Total Carbon Column Observing Network
879 (TCCON), Phil. Trans. R. Soc. A369, 2087-2112, doi: 10.1098/rsta.2010.0240, 2011.

880 76. Yang, Z., Washenfelder, R. a., Keppel-Aleks, G., Krakauer, N.Y., Randerson, J.T., Tans, P.P.,
881 Sweeney, C., and Wennberg, P.O.: New constraints on Northern Hemisphere growing season net
882 flux, Geophysical Research Letters, 34, 1–6, doi:10.1029/2007GL029742,
883 http://www.agu.org/pubs/crossref/2007/2007GL029742.shtml, 2007.

884 77. Yokota, T., Yoshida, Y., Eguchi, N., Ota, Y., Tanaka, T., Watanabe, H., and Maksyutov, S.:
885 Global concentrations of CO_2 and CH_4 retrieved from GOSAT: First preliminary results,
886 Scientific Online Letters on the Atmosphere (SOLA), 5, 160–163, doi:10.2151/sola.2009-041,
887 2009.

Table 1. *Levels of the vertical grid in the NIES TM model*

	H, km	$\sigma = P/P_s$	≈Δ, m	ζ (σ–θ grid levels), K	Number of levels
Near-surface layer	0-2	1.0–0.795	250	-	8
Free troposphere	2–12	0.795–0.195	1000	- 330, 350	10
Upper troposphere and stratosphere	12–40	0.195–0.003	1000 2000 –	365, 380, 400, 415, 435, 455, 475, 500 545, 590, 665, 850, 1325, 1710	14
				Total levels:	32

Table 2. *Locations of TCCON and GLOBALVIEW stations used in the comparisons*

No	TCCON stations			GLOBALVIEW stations			
	Station name	Lat.	Lon.	Station name	Lat.	Lon.	Alt., m
1	Bialystok	53.22°N	23.13°E	Baltik See	55.35°N	17.22°E	28
2	Bremen	53.10°N	8.85°E	Ocean Station M	66.00°N	2.00°E	5
3	Darwin	12.42°S	130.89°E	Darwin	12.42°S	130.57°E	3
4	Garmisch	47.48°N	11.06°E	Hohenpeissenberg	47.80°N	11.01°E	990
5	Izaña	28.30°N	16.50°W	Izaña	28.31°N	16.50°W	2360
6	Lamont	36.61°N	97.49°W	Southern Great Plains	36.80°N	97.50°W	374
7	Lauder	45.04°S	169.68°E	Baring Head	41.41°S	174.87°E	80
8	Orleans	47.97°N	2.11°E	Pic Du Midi	42.93°N	0.13°E	2877
9	Park Falls	45.95°N	90.27°W	Park Falls	45.95°N	90.27°W	483
10	Sodankylä	67.37°N	26.63°E	Pallas-Sammaltunturi	67.97°N	24.12°E	560
11	Tsukuba	36.05°N	140.12°E	Ryori BAPMon	39.03°N	141.83°E	260
12	Wollongong	34.41°S	150.88°E	Cape Grim	40.68°S	144.69°E	164
13				Alert	82.45°N	297.48°E	110
14				Mauna Loa	19.54°N	155.58°W	3397
15				Syowa	69.00°S	39.58°E	14

Table 3. *Correlation coefficients and biases of the modelled XCO_2 and XCH_4*

No	Station name	XCO_2		XCH_4	
		Correlation	Bias, ppm	Correlation	Bias, ppb
1	Bialystok (Poland, 53.22°N, 23.13°E)	0.93	0.61	0.74	4.52
2	Bremen (Germany, 53.10°N, 8.85°E)	0.88	0.19	0.72	1.27
3	Darwin (Australia, 12.42°S, 130.89°E)	0.90	-0.62	0.55	-2.41
4	Garmisch (Germany, 47.48°N, 11.06°E)	0.93	0.76	0.44	0.98
5	Izaña (Spain, 28.30°N, 16.50°W)	0.87	-0.53	0.53	9.05
6	Lamont (USA, 36.61°N, 97.49°W)	0.91	-0.44	0.62	-1.13
7	Lauder (New Zealand, 45.04°S, 169.68°E)	0.90	0.22	0.58	-1.20
8	Orleans (France, 47.97°N, 2.11°E),	0.96	0.17	0.59	-8.80
9	ParkFalls (USA, 45.95°N, 90.27°W)	0.95	-0.28	0.51	-2.30
10	Sodankylä (Finland, 67.37°N, 26.63°E)	0.94	1.21	0.40	20.91
11	Tsukuba (Japan, 36.05°N, 140.12°E)	0.85	-0.24	0.53	3.80
12	Wollongong (Australia, 34.41°S, 150.88°E)	0.80	0.32	0.66	-8.19
All stations		0.90	-0.62 (-0.16%) 1.21 (0.31%)	0.54	-8.80 (-0.49%) 20.91 (1.16%)

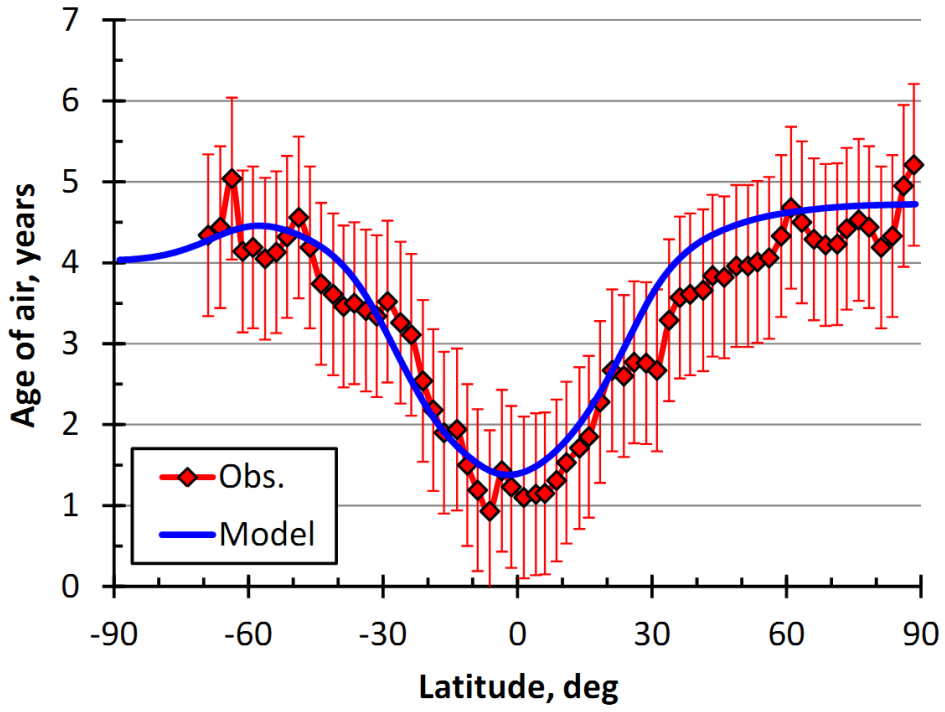

913

914 **Fig. 1.** Mean age of air at 20 km altitude from NIES TM simulations (blue line), compared with
915 the mean age of air derived from *in situ* ER-2 aircraft observations of CO_2 (Andrews et al.,
916 2001) and SF_6 (Ray et al., 1999) (red line). Error bars for the observations are 2σ
917 (Monge-Sanz et al., 2007).

918

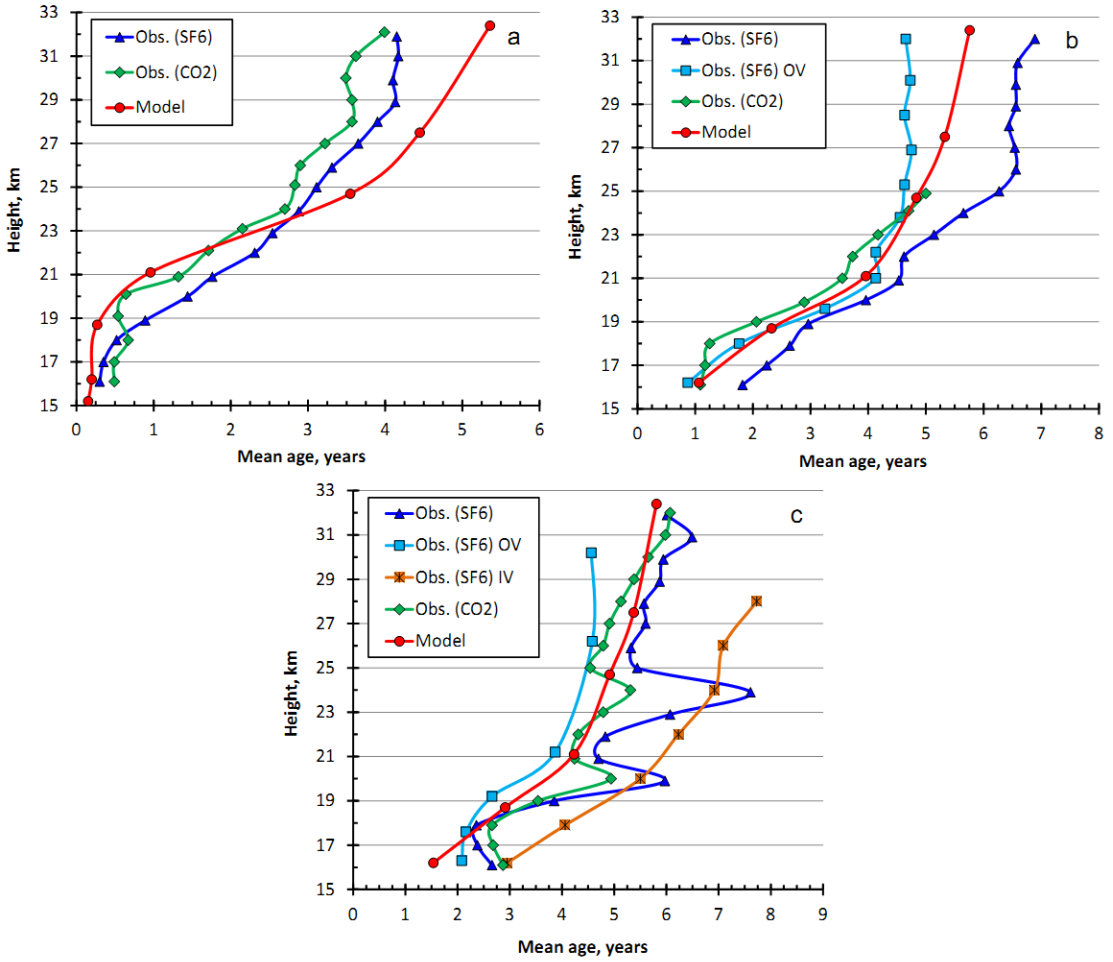

Fig. 2. Comparison of observed and modelled (red lines) mean age of air at latitudes of: (a) 5°S, (b) 40°N, and (c) 65°N. The lines with symbols represent observations: *in situ* SF_6 (dark blue line with triangles) (Elkins et al., 1996; Ray et al., 1999), whole air samples of SF_6 (light blue with square outside vortex, and orange line with asterisk inside vortex) (Harnisch et al., 1996), and mean age from *in situ* CO_2 (green line with diamonds) (Boering et al., 1996; Andrews et al., 2001).

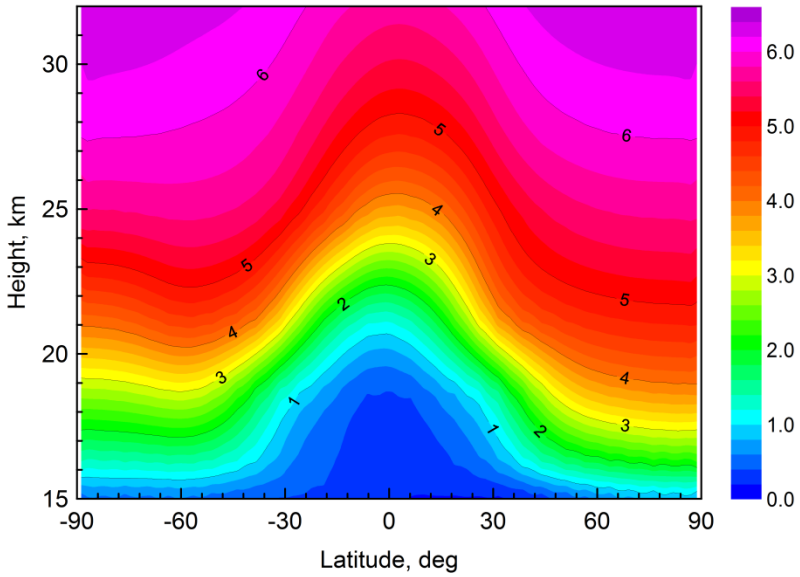

927

928 **Fig. 3.** Cross-section of the annual mean age of air (years) from NIES TM simulations of SF_6 with
929 JRA-25/JCDAS reanalysis.

930

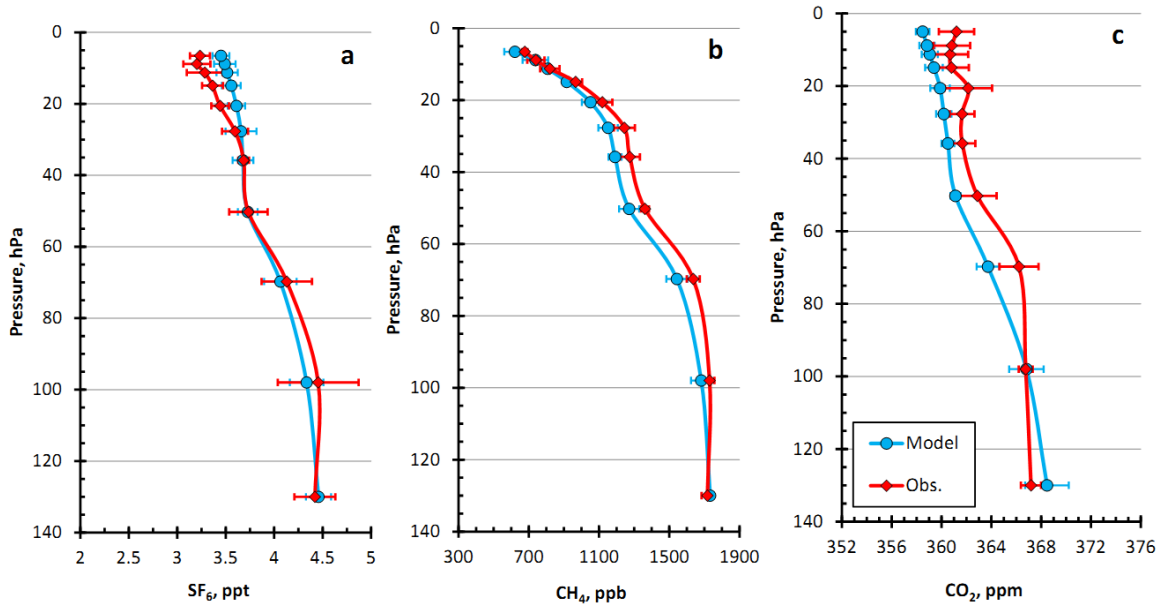

931

932 **Fig. 4.** Comparison of observed and modelled concentration averaged for the period 2000–2007: a)
933 SF_6, b) CH_4, and c) CO_2. The observed VMRs were derived from six individual profiles of
934 balloon-borne measurements over Sanriku, Japan (39.17°N, 141.83°E).

935

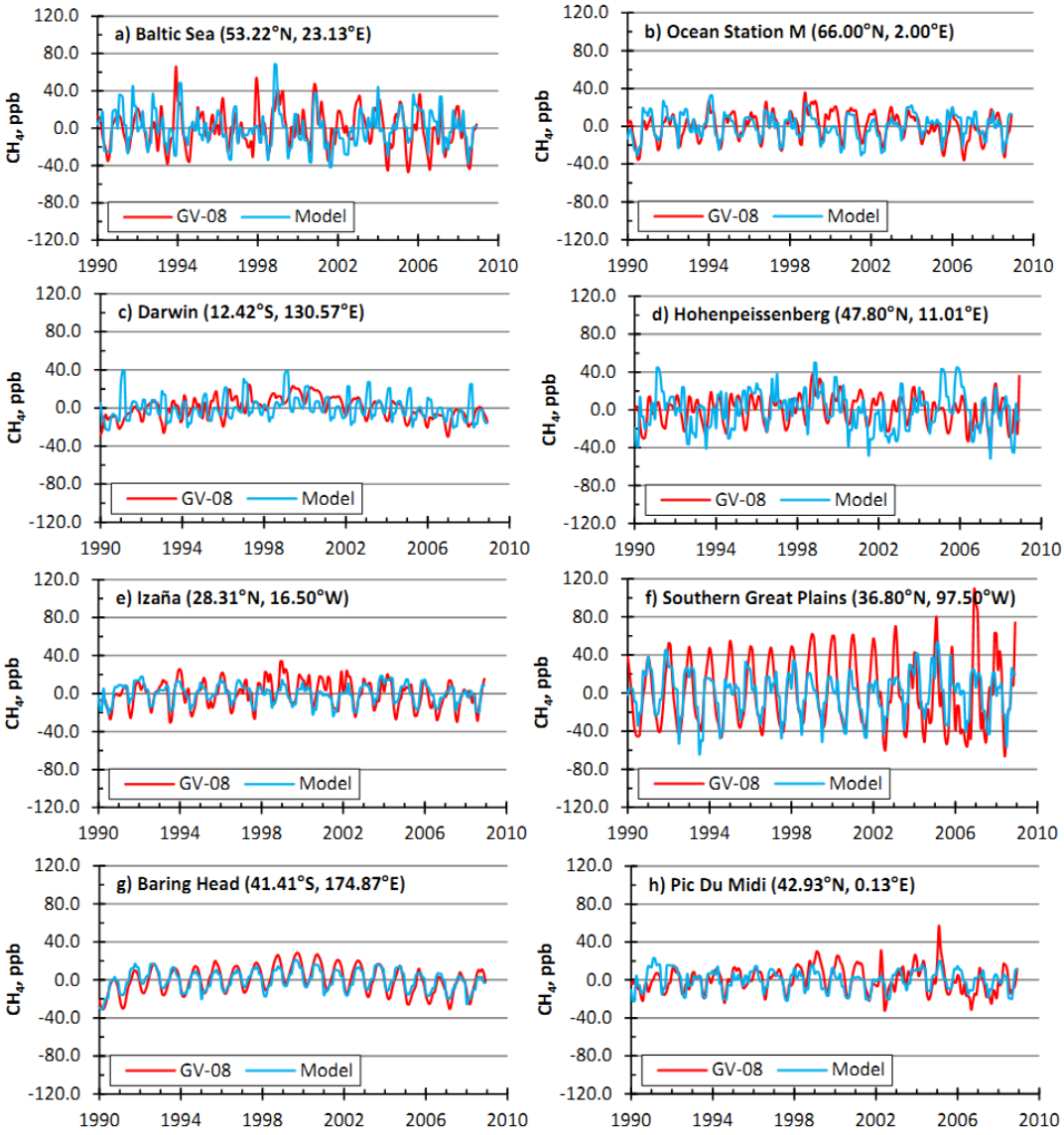
a) Baltic Sea (53.22°N, 23.13°E)
b) Ocean Station M (66.00°N, 2.00°E)
c) Darwin (12.42°S, 130.57°E)
d) Hohenpeissenberg (47.80°N, 11.01°E)
e) Izaña (28.31°N, 16.50°W)
f) Southern Great Plains (36.80°N, 97.50°W)
g) Baring Head (41.41°S, 174.87°E)
h) Pic Du Midi (42.93°N, 0.13°E)
CH4, ppb
120.0
80.0
40.0
0.0
-40.0
-80.0
-120.0
1990
1994
1998
2002
2006
2010
GV-08
Model

936

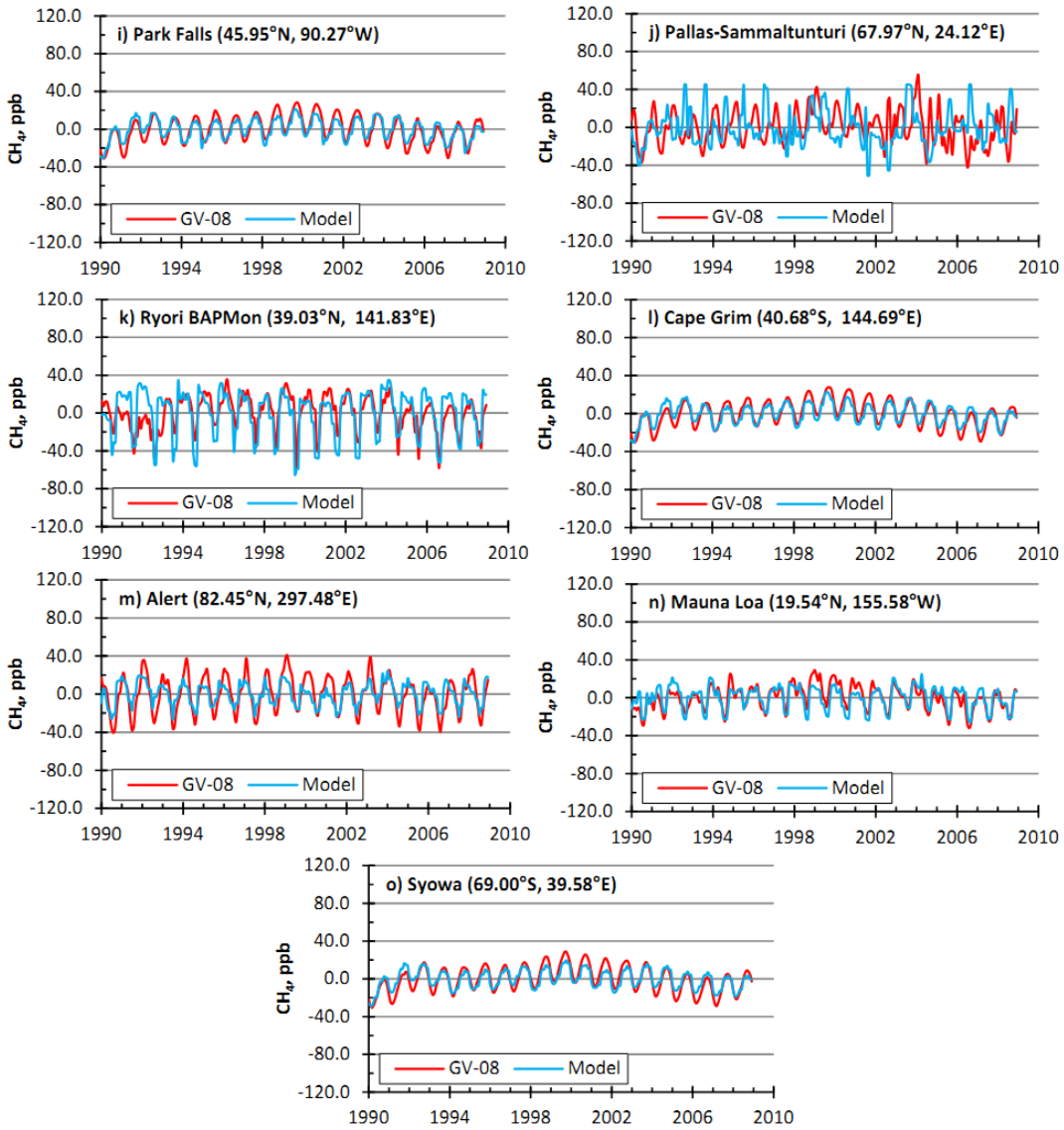

937

938 **Fig. 5.** Detrended seasonal cycle of CH_4 surface volume mixing ratio for GLOBALVIEW stations
939 (corresponding TCCON stations in parentheses): a) Baltik See (Bialystok); b) Ocean Station
940 M (Bremen); c) Darwin (Darwin); d) Hohenpeissenberg (Garmisch); e) Izaña (Izaña); f)
941 Southern Great Plains (Lamont); g) Baring Head Station (Lauder); h) Pic Du Midi
942 (Orleans); i) Park Falls (Park Falls); j) Pallas-Sammaltunturi (Sodankylä); k) Ryori
943 (Tsukuba); l) Cape Grim (Wollongong); m) Alert; n) Mauna Loa; and o) Syowa.

944

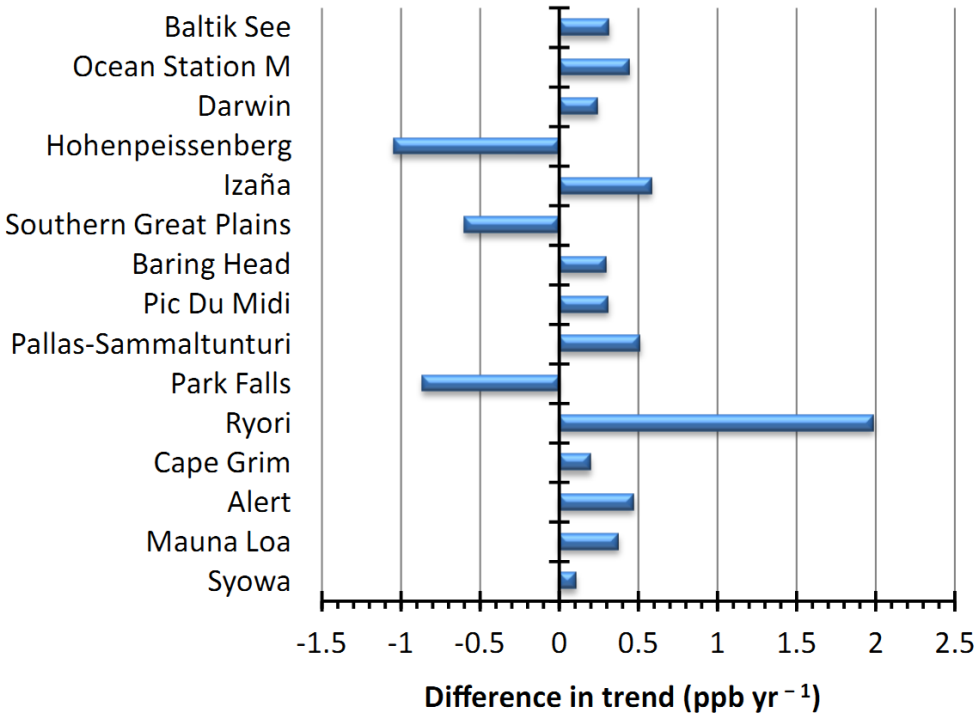

945

946 **Fig. 6.** Average difference between simulated and observed trends (ppb/yr) of CH_4 for Jan 1990
947 and Dec 2009 at GLOBALVIEW stations.

948

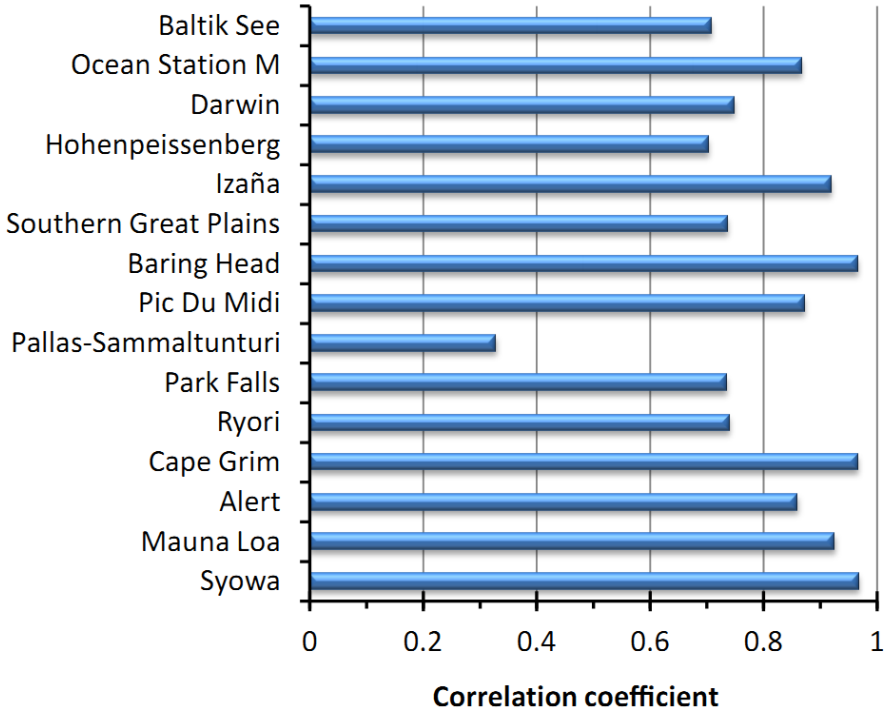

949

950 **Fig. 7.** Correlation coefficients between simulated and observed CH_4 at GLOBALVIEW stations.

951

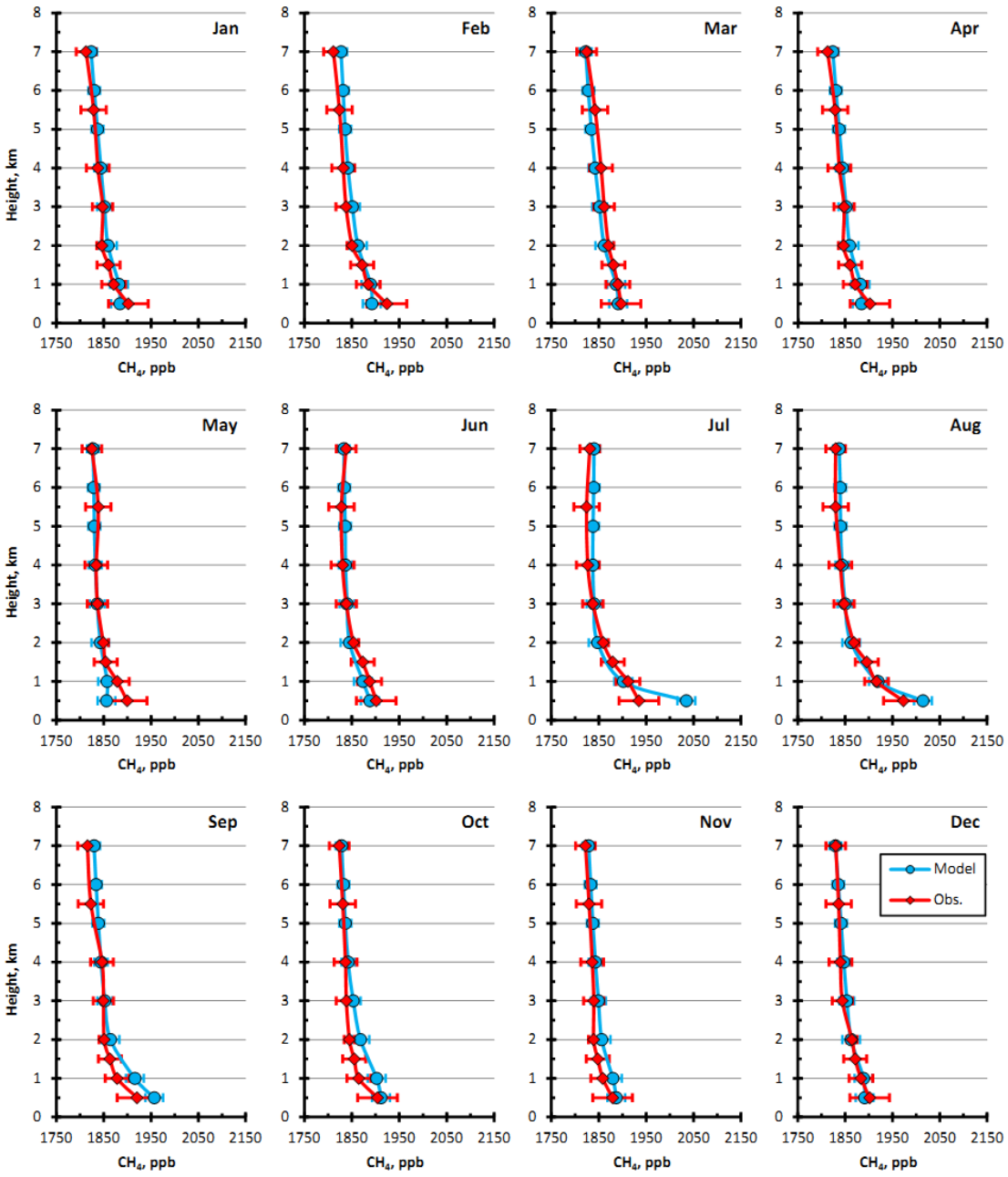

952

953 **Fig. 8.** Comparison of observed and modelled CH_4 concentrations averaged for the period 1993-
954 2007. The vertical profiles were produced by averaging the modelled and observed
955 concentrations taken on the same day and at the same time. Error bars show the standard
956 deviation.

957

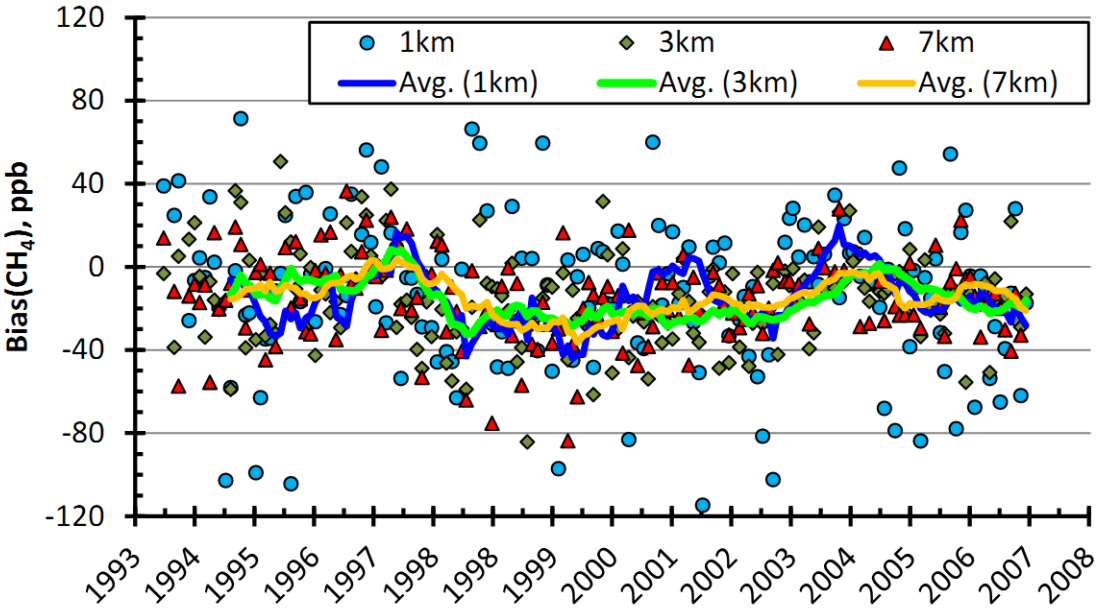

Fig. 9. Time series of bias (model minus observation) and the averaged (moving average with period 12) value of bias for the 1, 3, and 7 km levels over Surgut (61.25°N, 73.43°E) for the period 1993–2007.

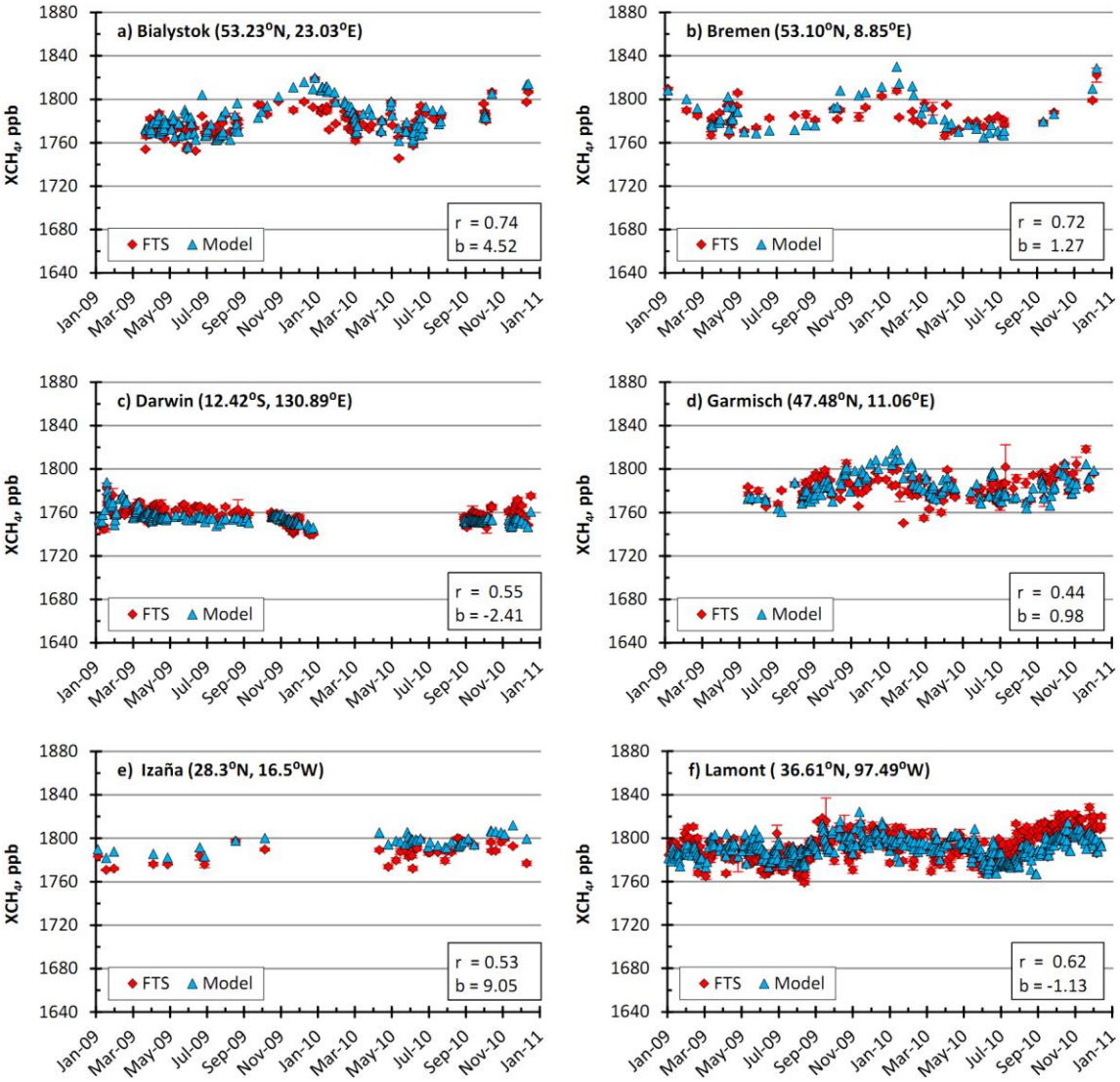
a) Bialystok (53.23°N, 23.03°E)
r = 0.74
b = 4.52
b) Bremen (53.10°N, 8.85°E)
r = 0.72
b = 1.27
c) Darwin (12.42°S, 130.89°E)
r = 0.55
b = -2.41
d) Garmisch (47.48°N, 11.06°E)
r = 0.44
b = 0.98
e) Izaña (28.3°N, 16.5°W)
r = 0.53
b = 9.05
f) Lamont (36.61°N, 97.49°W)
r = 0.62
b = -1.13
FTS
Model
XCH4, ppb
1880
1840
1800
1760
1720
1680
1640
Jan-09
Mar-09
May-09
Jul-09
Sep-09
Nov-09
Jan-10
Mar-10
May-10
Jul-10
Sep-10
Nov-10
Jan-11

963

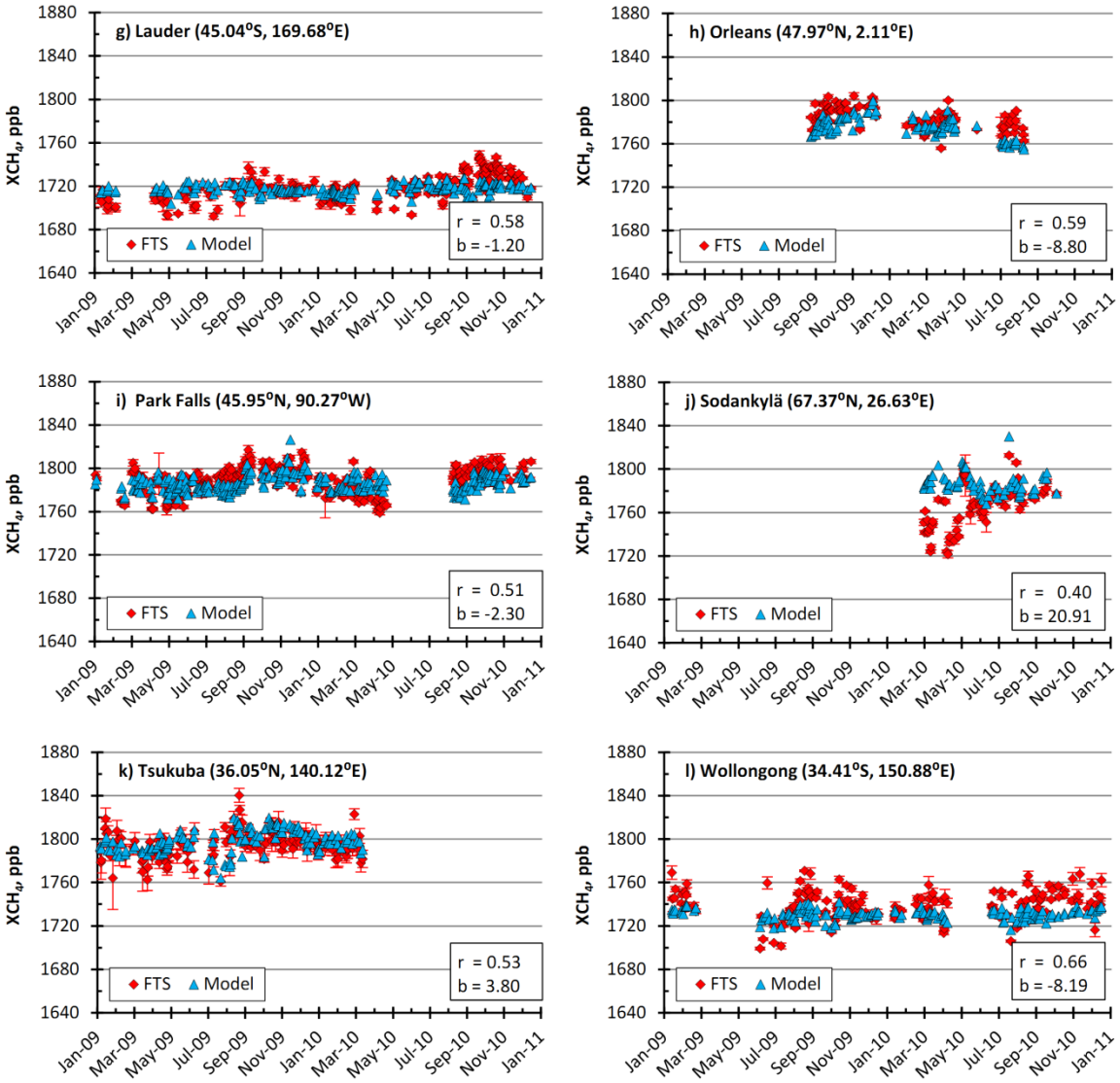

964

965 **Fig. 10.** Time series of XCH_4 measured by FTS and modelled by NIES TM for the period January
966 2009 to February 2011, for the following stations: a) Bialystok (Poland, 53.22°N, 23.13°E);
967 b) Bremen (Germany, 53.10°N, 8.85°E); c) Darwin (Australia, 12.42°S, 130.89°E); d)
968 Garmisch (Germany, 47.48°N, 11.06°E); e) Izaña (Spain, 28.30°N, 16.50°W); f) Lamont
969 (USA, 36.6°N, 97.49°W); g) Lauder (New Zealand, 45.04°S, 169.68°E); h) Orleans
970 (France, 47.97°N, 2.11°E); i) Park Falls (USA, 45.95°N, 90.27°W); j) Sodankylä (Finland,
971 67.37°N, 26.63°E); k) Tsukuba (Japan, 36.05°N, 140.12°E); and l) Wollongong (Australia,
972 34.41°S, 150.88°E). The "error" for each symbol is a combination of the spread due to
973 weighted averaging within the 13:00 ± 1 hour local time interval and observation error.

974

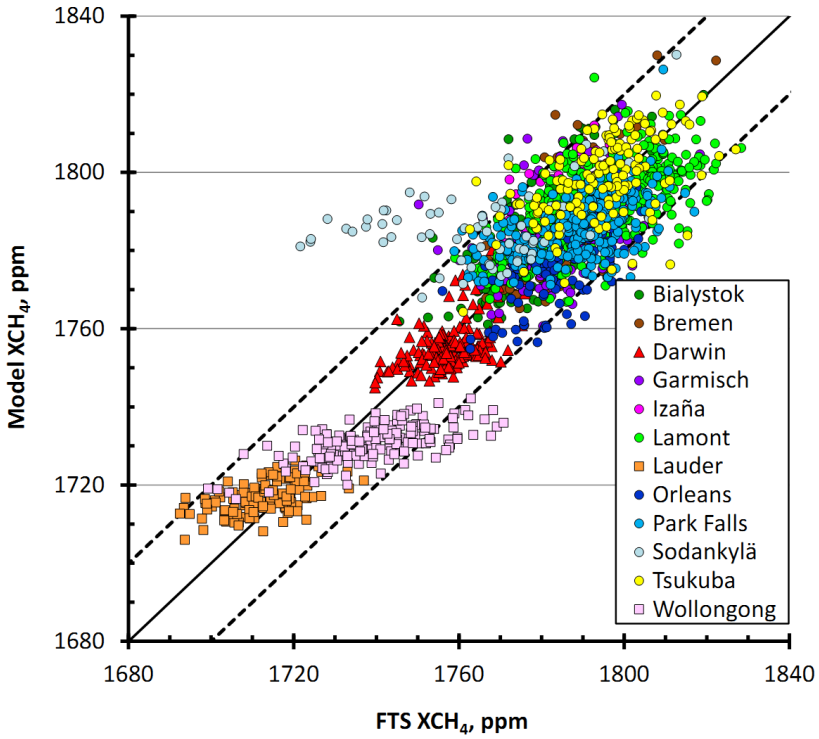

Fig. 11. Scatter diagram of modelled and FTS XCH_4 at all FTS sites. Dotted lines show a standard deviation of ±1% of XCH_4.

980

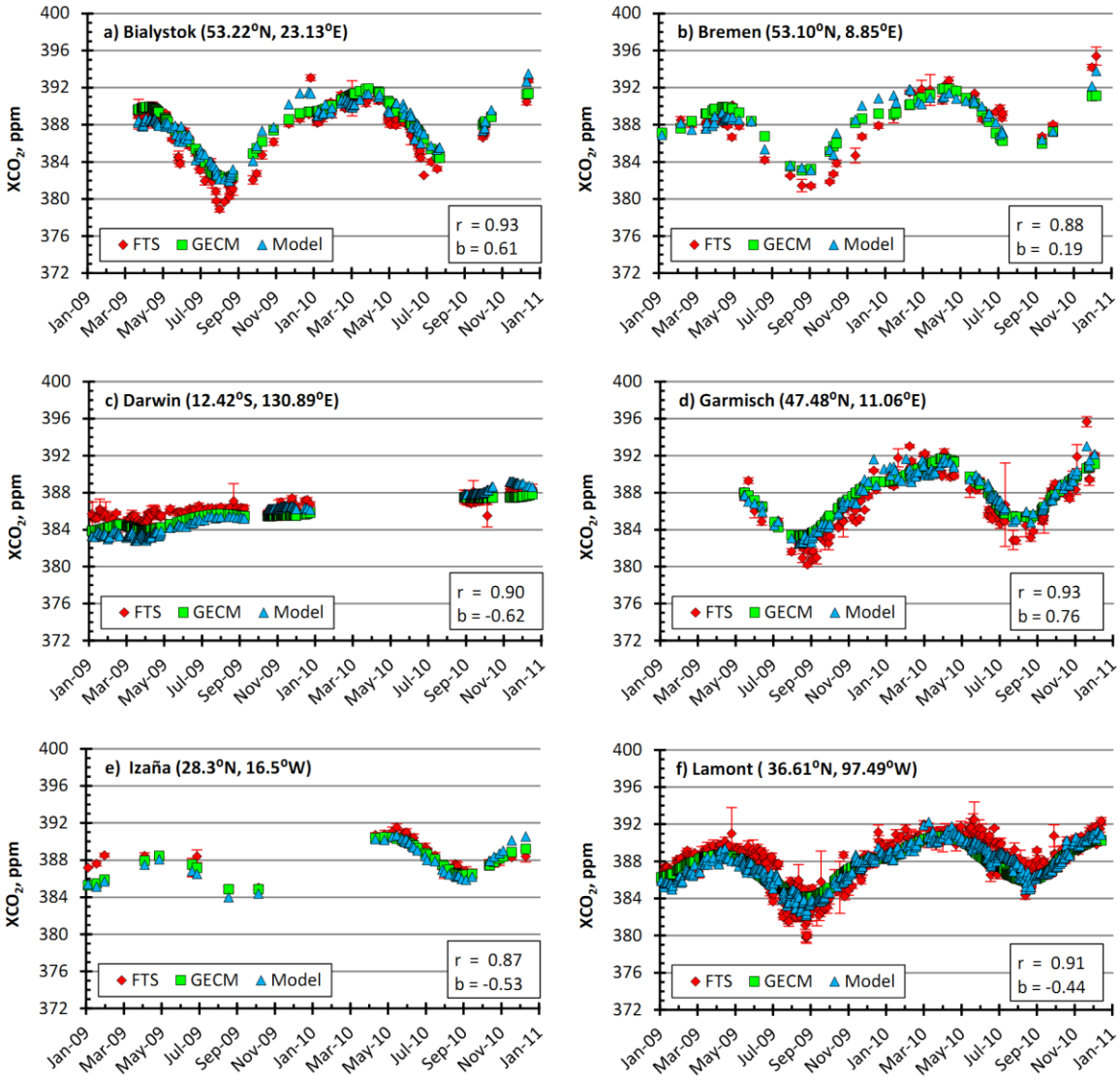
a) Bialystok (53.22°N, 23.13°E)
r = 0.93
b = 0.61
b) Bremen (53.10°N, 8.85°E)
r = 0.88
b = 0.19
c) Darwin (12.42°S, 130.89°E)
r = 0.90
b = -0.62
d) Garmisch (47.48°N, 11.06°E)
r = 0.93
b = 0.76
e) Izaña (28.3°N, 16.5°W)
r = 0.87
b = -0.53
f) Lamont (36.61°N, 97.49°W)
r = 0.91
b = -0.44
FTS
GECM
Model
XCO2, ppm
400
396
392
388
384
380
376
372
Jan-09
Mar-09
May-09
Jul-09
Sep-09
Nov-09
Jan-10
Mar-10
May-10
Jul-10
Sep-10
Nov-10
Jan-11

981

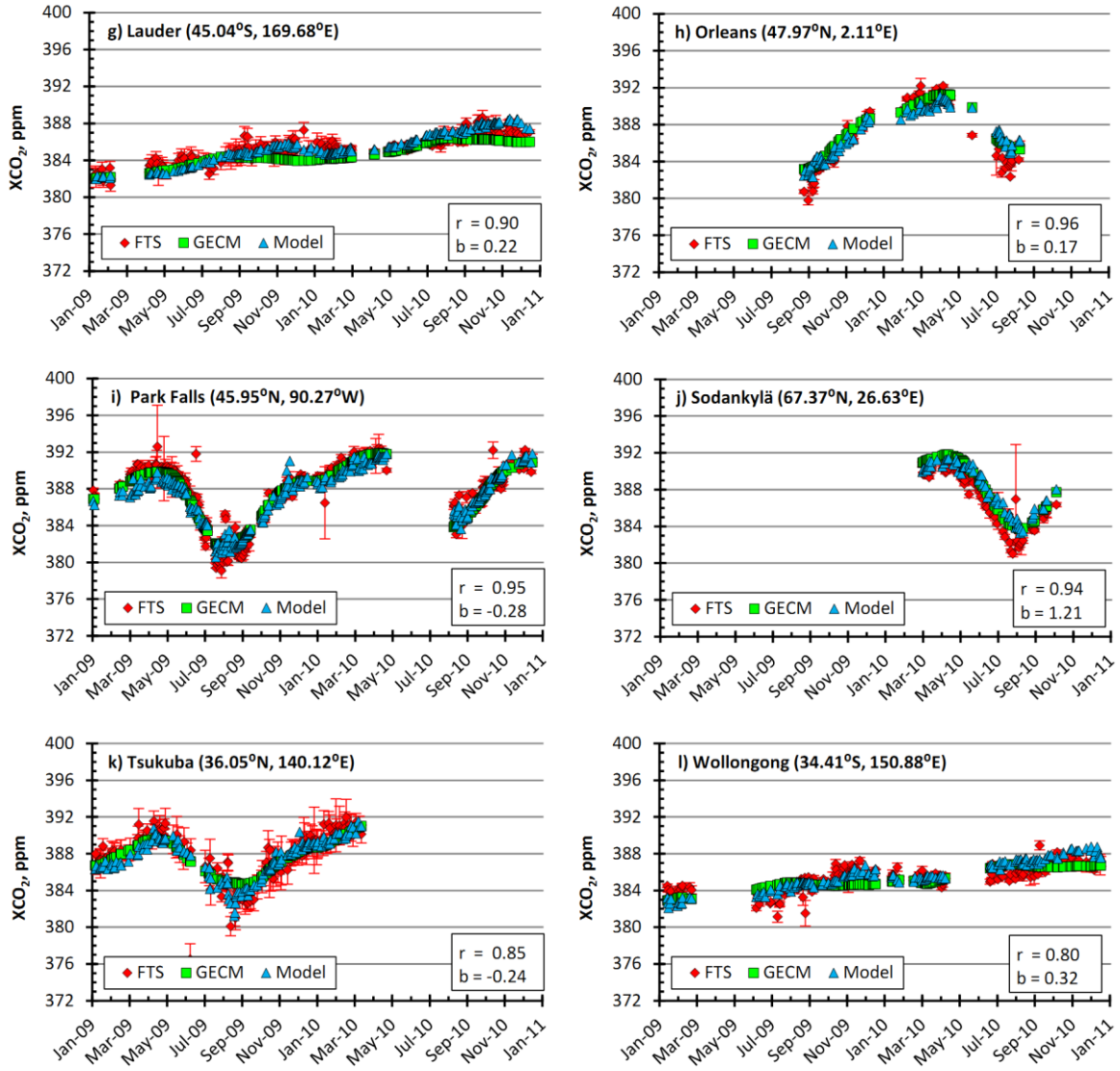

982

983

984 **Fig. 12.** Time series of XCO_2 measured by FTS, modelled by NIES TM and derived from a 3-D
985 CO_2 climatology GECM for the period January 2009 to February 2011, for the following
986 stations: a) Bialystok (Poland, 53.22°N, 23.13°E); b) Bremen (Germany, 53.10°N, 8.85°E);
987 c) Darwin (Australia, 12.42°S, 130.89°E); d) Garmisch (Germany, 47.48°N, 11.06°E);
988 e) Izaña (Spain, 28.30°N, 16.50°W); f) Lamont (USA, 36.6°N, 97.49°W); g) Lauder (New
989 Zealand, 45.04°S, 169.68°E); h) Orleans (France, 47.97°N, 2.11°E); i) Park Falls (USA,
990 45.95°N, 90.27°W); j) Sodankylä (Finland, 67.37°N, 26.63°E); k) Tsukuba (Japan,
991 36.05°N, 140.12°E); and l) Wollongong (Australia, 34.41°S, 150.88°E). The "error" for
992 each symbol is a combination of the spread due to weighted averaging within the 13:00 ± 1
993 hour local time interval and observation error.

994

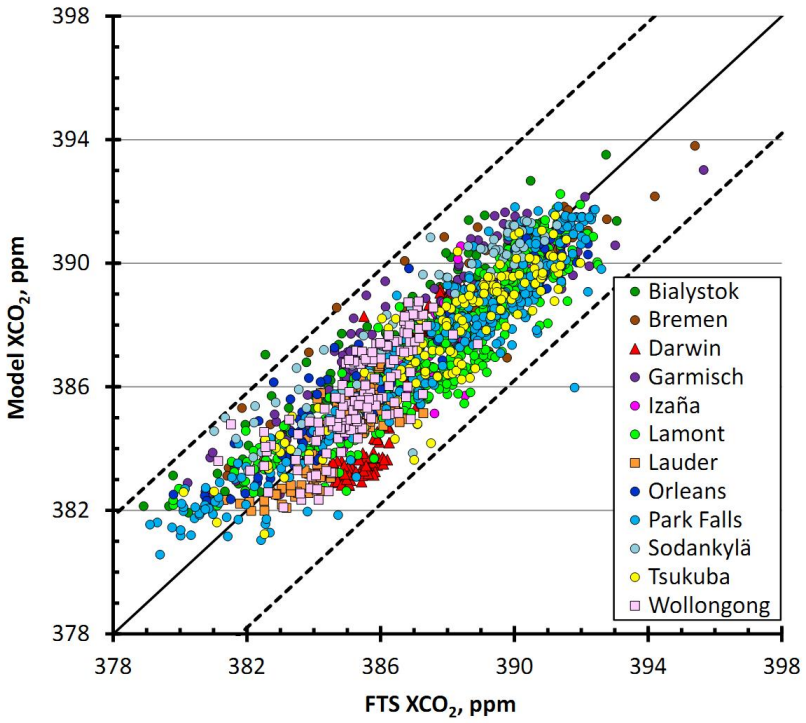

Fig. 13. As for Fig. 11, but for XCO_2.